

Response to Topical Editor (Dr. Fiona O'Connor)

We thank your insightful comments. We revised our manuscript accordingly.

1. The model source code is “freely available upon request”. This does not meet the requirements of the journal. If the source code is freely available, can you please archive it in accordance with GMD policy and update the code/data availability section of your manuscript? If it cannot be published, then you will need to indicate the licence conditions in the manuscript.

Response:

We have not finished the preparation of a user guide how to run the BCC-ESM1 model, and some source codes at the present version would be difficult for users to comprehend. So, we have modified the statements in section of “Code and data availability” as “The source codes of BCC-ESM1 model are available for use under licence agreement. Readers interested in BCC-ESM1 codes may contact Dr. Tongwen Wu (twwu@cma.gov.cn) for further details.”

2. Model outputs on ESGF is very good practice but can be difficult to find. ESGF provides the correct data citation for each piece of data on the corresponding catalogue page, so can I please ask that you precisely cite the data? Precise instructions for citing CMIP6 data are here: https://docs.google.com/document/d/1SnwBL9MJQNEU1_nJ661SN3-SSxR0j1mAYan6-WXfaSU/edit

Response: We have added the data citation for CMIP6 data on ESGF.

3. The model input files required to reproduce the simulations are not referred to. Again, may I please ask that you publicly archive these and update the code/data availability section accordingly?

Response: We have modified the statements as “Readers interested in BCC-ESM1 codes and the model input files required to reproduce the simulations may contact Dr. Tongwen Wu (twwu@cma.gov.cn) for further details.”

You can find full details of the requirements of the journal for model description papers at:

https://www.geoscientific-model-development.net/about/manuscript_types.html#item1

Thirdly, on reading the reviewer comments, your responses to them, and the revised manuscript, I feel that you have addressed the majority of comments from Reviewer #1 with one exception as follows.

Reviewer #1 raised an important point about the imbalance in the TOA radiative fluxes in BCC-ESM. Although you cite Wild et al. (2013) to support that such an imbalance is common among other models, the comparison of models and the observational dataset used in that paper is referring to the present day, in which case an imbalance would be expected. However, in a pre-industrial control experiment as described in your manuscript, there is little anthropogenic forcing and as such, the TOA is expected to be more in balance. You clearly show little drift in surface temperature and sea surface temperatures in your Figure 1 but can you confirm whether BCC-ESM is indeed conserving energy?

Response:

Yes, +0.7 Wm⁻² net energy flux at TOA in BCC-ESM1 means that BCC-ESM1 has not absolute energy balance in the whole system. So we added a sentence as “It means that there exists surplus energy of 0.7 Wm⁻² obtained by the whole system, but do not cause remarkable climate drift in BCC-ESM1.”

In relation to Reviewer #2, they had concerns about the level of detail in the description of the aerosol scheme and how it compared with other existing schemes, and noted that the evaluation of the scheme itself in BCC-ESM1 was mainly qualitative and when quantitative, referred to quite old references.

I think the additional comparisons that you’ve made (e.g. HIPPO, Taylor plot) and the inclusion of more quantitative measures of skill (e.g. Table 7) add to the quality of the evaluation and the manuscript.

Response: Following your suggestion, we have added quantitative evaluation for Black Carbon using HIPPO aircraft observations in Table 7. As HIPPO data spans a short time period, the Taylor plot is not made.

However, I would ask that you include information on the requested optical properties used (e.g. extinction co-efficient, asymmetry parameter etc..).

Response:

We have added a paragraph in section 2.5 to describe the information on requested optical properties of aerosols used. “The treatment of aerosol single scattering (optical) properties (such as mass extinction efficiency, single scattering albedo, and asymmetric factor) follows the look-up table approach in CAM [Collins et al., 2004]. The optics for black, organic carbon, sea salt, and sea salt particles is assumed to be same as the optics for soot and water-soluble aerosols in the Optical Properties of Aerosols and Clouds (OPAC) data set [Hess et al., 1998]. The optics for dust is derived by Mie calculations for the size distribution represented by each size bin [Zender et al., 2003]. Similarly, for sulfate and nitrate particles, same set of aerosol optical properties for ammonium sulfate are used and are taken from Wang

et al. [2008] with treatment of aerosol hygroscopicity. The volcanic stratospheric aerosols are assumed to be comprised of 75% sulfuric acid and 25% water, as in Hess et al. [1998]. For each model year, different aerosol types are assumed to be externally mixed in the calculation of bulk aerosol single scattering properties that are in turn used in the radiative transfer calculations.”

Finally, I also have a number of specific comments below that I ask you to implement.

Specific Comments:

1. When referring to GHGs, replace NO₂ with N₂O? (Line 86 of revised manuscript) and give full names e.g. nitrous oxide (N₂O)

Response: NO₂ has replaced by N₂O. Its full name appears first in line 52.

2. Please give complete names. As an example, replace CH₂O with “formaldehyde (CH₂O)” (Lines 142-144) and do likewise for all species referred to in the manuscript.

Response: Modified for all species.

3. Replace “Wet removals are ...” with “Wet removal ... is ...” (Line 138)

Response: Modified.

4. Please include appropriate references for CMIP6 biomass burning emissions, GHGs and solar forcing (e.g. van Marle et al., 2017)

Response: We have added the references of CMIP6 forcing data used in lines 315 to 326

5. The protocol for the CMIP6 coupled historical experiment is from Eyring et al. (2016). AerChemMIP (Collins et al., 2017) is using those historical ensemble members as controls for parallel sensitivity experiments. Please remove Collins et al. (2017) as the reference for the coupled historical simulation protocol (Line 307-308)

Response: Following your comment, to remove Collins et al. (2017) as the reference for the coupled historical simulation protocol. We have rewritten this sentence to “The historical experiment is forced with emissions evolving from 1850 to 2014 include biomass burning emissions (Van Marle et al. 2017), anthropogenic and open burning emissions (Hoesly et al., 2017; Hoesly et al., 2018; Feng et al., 2019)”

6. For N₂O and CH₄, it is still unclear whether they are only prescribed at the surface (and at the top boundary) and their concentrations in the remaining atmosphere are interactive. When you say “CH₄, N₂O, CO₂, CFC11, and CFC12 are prescribed using CMIP6 historical forcing data as suggestion in AerChemMIP protocol. Although CH₄ and N₂O are prognostic variables in the chemistry scheme (Table 1), their prognostic

values at each model step in the historical experiment are replaced by CMIP6 data“, are their concentrations replaced throughout the model domain or only at the surface and top boundary? Please clarify. Again here, Collins et al. (2017) and AerChemMIP are not the appropriate reference for the coupled historical protocol (Lines 310-313 and 378-380)

Response: The original purpose of our work is to follow the AerChemMIP described in Collins et al., (2017). The legend of Table 1 in Collins et al., (2017) is “... Models should always be run with the maximum complexity available. The species columns refer to the specifications for concentrations (CH₄, N₂O and CFC/HCFC) or emissions (aerosol and ozone precursors). “Hist” means the concentrations or emissions should evolve as for the CMIP6 historical simulation ...”.

We understand that as "concentrations of CH₄, N₂O, CFC are specified for the coupled historical experiment of AerChemMIP". Anyway, we have removed “as suggestion in AerChemMIP protocol” in lines 310 to 331 and “the reference of Collins et al. (2017) in line 318 to 320.

7. Give full name for ACCMIP (Line 333)

Response: Modified.

8. Change “eruption” to “eruptions” in Section heading (Line 354)

Response: Modified.

1 **Beijing Climate Center Earth System Model version 1 (BCC-ESM1):**

2 **Model Description and Evaluation of Aerosol Simulations**

3
4 **Tongwen Wu^{1*}, Fang Zhang¹, Jie Zhang¹, Weihua Jie¹, Yanwu Zhang¹, Fanghua Wu¹,**
5 **Laurent Li^{1,2}, Jinghui Yan¹, Xiaohong Liu³, Xiao Lu⁴, Haiyue Tan⁴, Lin Zhang⁴,**
6 **Jun Wang⁵, Aixue Hu⁶**

7
8 ¹Beijing Climate Center, China Meteorological Administration, Beijing, China

9 ²Laboratoire de M é t é o r o l o g i e D y n a m i q u e, I P S L, C N R S, S o r b o n n e U n i v e r s i t é E c o l e N o r m a l e
10 S u p é r i e u r e, E c o l e P o l y t e c h n i q u e, P a r i s, F r a n c e

11 ³Texas A&M University, College Station, TX, USA

12 ⁴Laboratory for Climate and Ocean-Atmosphere Studies, Department of Atmospheric and
13 Oceanic Sciences, School of Physics, Peking University, Beijing, China

14 ⁵University of Iowa, Iowa City, IA 52242, USA

15 ⁶National Center for Atmospheric Research, PO Box 3000, Boulder, Colorado 80307-3000,
16 USA

17
18
19
20 *Correspondence to:* Tongwen Wu (twwu@cma.gov.cn)

21
22 Submit to Geosci. Model Dev.

23
24 **Revised on Oct. 23, 2019**

25 **Revised on Dec. 14, 2019**

26

27 **Abstract.** BCC-ESM1 is the first version of a fully-coupled Earth System Model with
28 interactive atmospheric chemistry and aerosols developed by the Beijing Climate Center,
29 China Meteorological Administration. Major aerosol species (including sulfate, organic
30 carbon, black carbon, dust and sea salt) and greenhouse gases are interactively simulated with
31 a whole panoply of processes controlling emission, transport, gas-phase chemical reactions,
32 secondary aerosol formation, gravitational settling, dry deposition, and wet scavenging by
33 clouds and precipitation. Effects of aerosols on radiation, cloud, and precipitation are fully
34 treated. The performance of BCC-ESM1 in simulating aerosols and their optical properties is
35 comprehensively evaluated as required by the Aerosol Chemistry Model Intercomparison
36 Project (AerChemMIP), covering the preindustrial mean state and time evolution from 1850
37 to 2014. The simulated aerosols from BCC-ESM1 are quite coherent with
38 CMIP5-recommended data, in-situ measurements from surface networks (such as IMPROVE
39 in the U.S. and EMEP in Europe), and aircraft observations. A comparison of modeled
40 aerosol optical depth (AOD) at 550 nm with satellite observations retrieved from Moderate
41 Resolution Imaging Spectroradiometer (MODIS) and Multi-angle Imaging
42 SpectroRadiometer (MISR) and surface AOD observations from AErosol RObotic NETwork
43 (AERONET) shows reasonable agreements between simulated and observed AOD. However,
44 BCC-ESM1 shows weaker upward transport of aerosols from the surface to the middle and
45 upper troposphere, likely reflecting the deficiency of representing deep convective transport
46 of chemical species in BCC-ESM1. With an overall good agreement between BCC-ESM1
47 simulated and observed aerosol properties, it demonstrates a success of the implementation of
48 interactive aerosol and atmospheric chemistry in BCC-ESM1.

49

50 **1. Introduction**

51 Atmosphere is a thin gaseous layer around the Earth, consisting of nitrogen, oxygen and
52 a large number of trace gases including important greenhouse gases (GHG) such as water
53 vapor, tropospheric ozone (O_3), carbon dioxide (CO_2), methane (CH_4), nitrous oxide (N_2O),
54 and chloro-fluoro-carbons (CFCs). Besides gaseous components, atmosphere also contains
55 various aerosols, which are important for cloud formation and radiative transfer. Atmospheric
56 trace gases and aerosols are actually interactive components of the climate system. Their
57 inclusion in global climate models (GCMs) is a significant enhancement for most
58 state-of-the-art climate models (Lamarque et al., 2013; Collins et al., 2017). Early attempts in
59 coupling global climate dynamics with atmospheric chemistry can be traced back to late
60 1970s, when 3D transport of ozone and simple stratospheric chemistry were firstly
61 incorporated into a GCM to simulate global O_3 production and transport (e.g., Cunnold et al.
62 1975; Schlesinger and Mintz 1979). Since mid-1980s, a large number of on-line global
63 climate/chemistry models have been developed to address issues of the Antarctic stratospheric
64 O_3 depletion (e.g., Cariolle et al. 1990; Austin et al. 1992; Solomon, 1999), tropospheric O_3
65 and sulfur cycle (e.g., Feichter et al. 1996; Barth et al. 2000), tropospheric aerosol and its
66 interactions with cloud (e.g., Chuang et al. 1997; Lohmann et al. 2000; Ghan and Easter, 2006;
67 Jacobson 2012). Aerosols and chemically reactive gases in the atmosphere exert important
68 influences on global and regional air quality and climate (Collins et al., 2017).

69 Since 2013, the Beijing Climate Center (BCC), China Meteorological Administration,
70 has continuously developed and updated its fully-coupled GCM, the Beijing Climate Center
71 Climate System Model (BCC-CSM) (Wu et al., 2013; Wu et al., 2014; Wu et al., 2019).
72 BCC-CSM version 1.1 was one of the comprehensive carbon-climate models participating in
73 the phase five of the Coupled Model Intercomparison Project (CMIP5, Taylor et al. 2012).
74 When forced by prescribed historical emissions of CO_2 from combustion of fossil fuels and
75 land use change, BCC-CSM1.1 successfully reproduced the trends of observed atmospheric
76 CO_2 concentration and global surface air temperature from 1850 to 2005 (Wu et al., 2013).
77 During recent years, BCC-CSM1.1 has been used in numerous investigations on soil organic
78 carbon changes (e.g. Todd-Brown et al., 2014), ocean biogeochemistry changes (e.g. Mora et
79 al., 2013), and carbon-climate feedbacks (e.g. Arora et al., 2013; Hoffman et al., 2014).

80 BCC-CSM includes main climate-carbon cycle processes (Wu et al., 2013) and the global
81 mean atmospheric CO₂ concentration is calculated from a prognostic equation of CO₂ budget
82 taking into account global anthropogenic CO₂ emissions and interactive land-atmosphere and
83 ocean-atmosphere CO₂ exchanges.

84 In recent years, BCC has put large efforts in developing a global
85 climate-chemistry-aerosol fully-coupled Earth System Model (BCC-ESM1) on the basis of
86 BCC-CSM2 (Wu et al., 2019). The objective is to interactively simulate global aerosols (e.g.
87 sulfate, black carbon, etc.) and main greenhouse gases (e.g. O₃, CH₄, N₂O₂ and CO₂) in the
88 atmosphere and to investigate feedbacks between climate and atmospheric chemistry.
89 BCC-ESM1 is at the point to be publicly released, and it is actively used by BCC for several
90 CMIP6-endorsed research initiatives (Eyring et al. 2016), including the Aerosol Chemistry
91 Model Intercomparison Project (AerChemMIP, Collins et al., 2017) and the Coupled
92 Climate–Carbon Cycle Model Intercomparison Project (C4MIP, Jones et al. 2016).

93 The purpose of this paper is to evaluate the performance of BCC-ESM1 in simulating
94 aerosols and their optical properties in the 20th century. The description of BCC-ESM1 is
95 presented in Section 2. The experimental protocol is given in Section 3. Section 4 presents the
96 evaluations of aerosol simulations with comparisons to CMIP5-recommended data (Lamarque
97 et al., 2010) and data obtained from both global surface networks and satellite observations.
98 The regional and global characteristics compared to observations and estimates from other
99 studies are analyzed. Simulations of aerosol optical properties in the 20th century are also
100 analyzed in Section 4. Conclusions and discussions are summarized in Section 5. Information
101 about code and data availability is given in Section 6.

102 **2. Model description**

103 BCC-ESM1 is an Earth System Model with interactive chemistry and aerosol
104 components, in which the atmospheric component is BCC Atmospheric General Model
105 version 3 (Wu et al., 2019) with interactive atmospheric chemistry (hereafter
106 BCC-AGCM3-Chem), land component BCC Atmosphere and Vegetation Interaction Model
107 version 2.0 (hereafter BCC-AVIM2.0), ocean component Modular Ocean Model version 4
108 (MOM4)-L40, and sea ice component [sea ice simulator (SIS)]. Different components of
109 BCC-ESM1 are fully coupled and interact with each other through fluxes of momentum,

110 energy, water, carbon and other tracers at their interfaces. The coupling between the
111 atmosphere and the ocean is done every hour.

112 The atmospheric component BCC-AGCM3-Chem is able to simulate global atmospheric
113 composition and aerosols from anthropogenic emissions as forcing agents. Its resolution is T42
114 (approximately $2.8125 \times 2.8125^\circ$ transformed spectral grid). The model has 26 levels in a hybrid
115 sigma/pressure vertical coordinate system with the top level at 2.914 hPa. Details of the model
116 physics are described in Wu et al. (2019). The BCC-AGCM3-Chem combines 66 gas-phase
117 chemical species and 13 bulk aerosol compounds as listed in Table 1. Apart from 3 gas-phase
118 species of dimethyl sulfide (DMS), sulfur dioxide (SO₂) and ammonia (NH₃), the other 63
119 gas-phase species are the same as those in the “standard version” of MOZART2 (Model for
120 Ozone and Related chemical Tracers, version 2), a global chemical transport model for the
121 troposphere developed by the National Center for Atmospheric Research (NCAR) driven by
122 meteorological fields from either climate models or assimilations of meteorological
123 observations (Horowitz et al., 2003). Advection of all tracers in BCC-AGCM3-Chem is
124 performed through a semi-Lagrangian scheme (Williamson and Rasch, 1989), and vertical
125 diffusion within the boundary layer follows the parameterization of Holtslag and Boville
126 (1993). The gas-phase chemistry of the 63 MOZART2 gas-phase species as listed in Table 1
127 is treated in the same way as that in the “standard version” of MOZART2 (Horowitz et al.,
128 2003), and there are 33 photolytic reactions and 135 chemical reactions involving 30 dry
129 deposited chemical species and 25 soluble gas-phase species. Dry deposition velocities for the
130 15 trace gases including O₃, carbon monoxide (CO), CH₄, formaldehyde (CH₂O), acetic acid
131 (CH₃OOH), hydrogen peroxide (H₂O₂), nitrogen dioxide (NO₂), nitric acid (HNO₃),
132 polyacrylonitrile (PAN), acetone (CH₃COCH₃), peroxyacetic acid (CH₃COOOH),
133 acetaldehyde (CH₃CHO), methylglyoxal (CH₃COCHO), nitric oxid (NO), and pernitric acid
134 (HNO₄) are not computed interactively and directly interpolated from MOZART2
135 climatological monthly mean deposition velocities
136 ([https://en.wikipedia.org/wiki/MOZART\(model\)](https://en.wikipedia.org/wiki/MOZART(model))) which are calculated offline (Bey et al., 2001;
137 Shindell et al., 2008) using a resistance-in-series scheme originally described in Wesely
138 (1989). The dry deposition velocities for the other 15 species including peroxy acetyl nitrate
139 (PAN), methyl nitroacetate (ONIT), organic nitrates (ONITR), ethyl alcohol (C₂H₅OH), organic

140 hydroxiperoxide (POOH), ethyl hydroperoxide (C₂H₅OOH), propylhydroperoxide
141 (C₃H₇OOH), methylene glycol mono acetate (ROOH), glycolaldehyde (GLYALD), acetyl
142 (HYAC), methanol (CH₃OH), propanoic acid (MACROOH), isoprene hydroxy hydroperoxide
143 (ISOPOOH), carboxylic acid (XOOH), formaldehyde (HYDRALD), and hydrogen (H₂) are
144 calculated using prescribed deposition velocities of O₃, CO, CH₃CHO, or land surface type
145 and surface temperature following the MOZART2 (Horowitz et al., 2003). Wet removals by
146 in-cloud scavenging for 25 soluble gas-phase species in the “standard version” of MOZART2
147 uses the parameterization of Giorgi and Chameides (1985) based on their temperature
148 dependent effective Henry’s law constants. In-cloud scavenging is proportional to the amount
149 of cloud condensate converted to precipitation, and the loss rate depends on the amount of
150 cloud water, the rate of precipitation formation, and the rate of tracer uptake by the liquid
151 phase water. Other highly soluble species such as HNO₃, H₂O₂, ONIT, ISOPOOH,
152 MACROOH, XOOH, and lead (Pb-210) are also removed by below-cloud washout as
153 calculated using the formulation of Brasseur et al. (1998). Below-cloud scavenging is
154 proportional to the precipitation flux in each model layer and the loss rate depends on the
155 precipitation rate. Vertical transport of gas tracers and aerosols due to deep convection is not
156 yet included in the present version of BCC-AGCM3-Chem, which process is considered as a
157 part of the deep convection and occurs generally in a small spatial region on a GCM-box with
158 low-resolution (2.8 lat. × 2.8 lon.). Another consideration is that a large uncertainty exists to
159 treat transport of those water-soluble tracers by deep convection. But this effect will be
160 involved in the next version of BCC model.

161 The BCC-AVIM2.0 is the land model with terrestrial carbon cycle. It is described in
162 details in Li et al. (2019) and includes biophysical, physiological, and soil carbon-nitrogen
163 dynamical processes. The terrestrial carbon cycle operates through a series of biochemical
164 and physiological processes on photosynthesis and respiration of vegetation. Biogenic
165 emissions from vegetation are computed online in BCC-AVIM2.0 following the algorithm of
166 the Model of Emissions of Gases and Aerosols from Nature version 2.1 (MEGAN2.1,
167 Guenther et al., 2012).

168 The oceanic component of BCC-ESM1 is the Modular Ocean Model version 4 with 40
169 levels (hereafter MOM4-L40), and the sea ice component Sea Ice Simulator (SIS).

170 MOM4-L40 uses a tripolar grid of horizontal resolution with 1 °longitude by 1/3 °latitude
171 between 30 S and 30 N ranged to 1 °longitude by 1 °latitude from 60 S and 60 N poleward
172 and 40 z-levels in the vertical. Carbon exchange between the atmosphere and the ocean are
173 calculated online in MOM4-L40 using a biogeochemistry module that is based on the
174 protocols from the Ocean Carbon Cycle Model Intercomparison Project–Phase 2 (OCMIP2,
175 <http://www.ipsl.jussieu.fr/OCMIP/phase2/>). SIS has the same horizontal resolution as
176 MOM4-L40 and three layers in the vertical, including one layer of snow cover and two layers
177 of equally sized sea ice. Details of oceanic component MOM4-L40 and sea-ice component
178 SIS that are used in BCC-ESM1 may be found in Wu et al. (2013) and Wu et al. (2019).

179 In the following sub-sections, we will describe the treatments in BCC-ESM1 for 3
180 gas-phase species of DMS, SO₂ and NH₃, 13 prognostic aerosol species including sulfate
181 (SO₄²⁻), 2 types of organic carbon (hydrophobic OC1, hydrophilic OC2), 2 types of black
182 carbon (hydrophobic BC1, hydrophilic BC2), 4 categories of soil dust (DST01, DST02,
183 DST03, DST04), and 4 categories of sea salt (SSLT01, SSLT02, SSLT03, SSLT04).
184 Concentrations of all aerosols in BCC-ESM1 are mainly determined by advective transport,
185 emission, dry deposition, gravitational settling, and wet scavenging by clouds and
186 precipitation, except for SO₄²⁻ which gas-phase and aqueous phase conversion from SO₂ are
187 also considered. The present version of aerosol scheme belongs to a bulk aerosol model and
188 mainly refers to the scheme of CAM-Chem (Lamarque et al., 2012), but the nucleation and
189 coagulation of aerosols are still ignored.

190 **2.1 SO₂, DMS, NH₃, and Sulfate**

191 SO₂ is a main sulfuric acid precursor to form aerosol sulfate SO₄²⁻. Conversions of SO₂
192 to SO₄²⁻ occur by gas phase reactions (Table 2) and by aqueous phase reactions in cloud
193 droplets. The dry deposition velocity of SO₂ follows the resistance-in-series approach of
194 Wesely (1989) using the formula, $W_{\text{SO}_2} = 1/(r_a + r_b + r_c)$, in which r_a , r_b , and r_c are the
195 aerodynamic resistance, the quasi-laminar boundary layer resistance, and the surface
196 resistance, respectively and they are interactively computed in each model time step. The loss
197 rate of SO₂ due to wet deposition is computed following the scheme in the global Community
198 Atmosphere Model (CAM) version 4, the atmospheric component of the Community Earth
199 System Model (Lamarque et al., 2012).

200 The sources of SO₂ mainly come from fuel combustion, industrial activities, and
201 volcanoes. SO₂ can also be formed from the oxidation of DMS as listed in Table 2 in which
202 their reaction rates follow CAM-Chem (Lamarque et al. 2012). The main source of DMS is
203 from oceanic emissions via biogenic processes. It is prescribed with the climatological
204 monthly data that are extracted from MOZART2 package
205 (<https://www2.acom.ucar.edu/gcm/mozart-4>). SO₄²⁻ is one of the prognostic aerosols in
206 BCC-AGCM3-Chem. Its treatment follows CAM4-Chem (Lamarque et al., 2012). It is
207 produced primarily by the gas-phase oxidation of SO₂ (in Table 2) and by aqueous phase
208 oxidation of SO₂ in cloud droplets. The gas phase reactions, rate constants, and gas-aqueous
209 equilibrium constants are given by Tie et al. (2001). The heterogeneous reactions of SO₄²⁻
210 occur on all aerosol surfaces. Their treatment follows a Bulk Aerosol Model (BAM) used in
211 CAM4 (Neale et al., 2010). The heterogeneous reactions depend strongly on pH values in
212 clouds which are calculated from the concentrations of SO₂, HNO₃, H₂O₂, NH₃, O₃, HO₂, and
213 SO₄²⁻. NH₃ is a gas tracer apart from MOZART2 (Table 1). Its sources include aircraft and
214 surface emissions due to anthropogenic activity, biomass burning, and biogenic emissions
215 from land soil and ocean surfaces (Table 4). SO₄²⁻ is assumed to be all in aqueous phase due
216 to water uptake, although Wang et al. (2008a) showed that ~34% of sulfate particles are in
217 solid phase globally due to the hysteresis effect of ammonium sulfate phase transition.
218 However, in terms of radiative forcing, consideration of solid sulfate formation process
219 lowers the sulfate forcing by ~8% as compared to consideration of all sulfate particles in
220 aqueous phase (Wang et al., 2008b). Future model development may consider the life cycle of
221 NH₃. The sulfate in- and below-cloud scavenging follows Neu and Prather (2011). Washout
222 of SO₄²⁻ is set to 20% of the washout rate of HNO₃ following Tie et al. (2005) and Horowitz
223 (2006). Dry deposition velocity of SO₄²⁻ is also calculated by the resistance-in-series
224 approach.

225 **2.2 Aerosols of organic carbon and black carbon**

226 BCC-AGCM3-Chem treats two types of organic carbon (OC), i.e. water-insoluble tracer
227 OC1 and water-soluble tracer OC2, and two types of black carbon (BC), i.e. water-insoluble
228 tracer BC1 and water-soluble tracer BC2. As shown in Table 2, hydrophobic BC1 and OC1
229 can be converted to hydrophilic BC2 and OC2 with a constant rate of $7.1 \times 10^{-6} \text{ s}^{-1}$ (Cooke and

230 Wilson, 1996). The 4 tracers of organic carbon and black carbon are mainly from emissions
231 including both fossil fuel and biomass burning, and are from the CMIP6 data package
232 (<https://esgf-node.llnl.gov/search/input4mips/>, Hoesly et al., 2018). Beside anthropogenic and
233 biomass burning emissions, hydrophilic organic carbon OC2 can also come from natural
234 biogenic volatile organic compound (VOC) emissions. Dry deposition velocities for all the 4
235 OC and BC tracers are set to $0.001\text{m}\cdot\text{s}^{-1}$. OC2 and BC2 are soluble aerosols, and their sinks
236 are primarily governed by wet deposition. Their in- and below-cloud scavenging follows the
237 scheme of Neu and Prather (2011).

238 **2.3 Sea salt aerosols**

239 As shown in Table 3, sea salt aerosols in the model are classified into four size bins (0.2–
240 1.0, 1.0–3.0, 3.0–10, and 10–20 μm) in diameter. They originate from oceans and are
241 calculated online by BCC-ESM1. The upward flux $F_{sea-salt}$ of sea salt productions for four
242 bins is proportional to the 3.41 power of the wind speed u_{10m} at 10 m height near the sea
243 surface (Mahowald et al., 2006) and is expressed as

$$244 \quad F_{sea-salt} = S \cdot (u_{10m})^{3.41}, \quad (1)$$

245 where S is a scaling factor and set to 4.05×10^{-15} , 4.52×10^{-14} , 1.15×10^{-13} , 1.20×10^{-13} for four
246 size bins of sea salt aerosols in BCC-ESM1, respectively.

247 Dry deposition of sea salts depends on the turbulent deposition velocity in the lowest
248 atmospheric layer using aerodynamic resistance and the friction velocity, and the settling
249 velocity through the whole atmospheric column for each bin of sea salts. The turbulent
250 deposition velocity and settling velocity depend on particle diameter and density (listed in
251 Table 3). In addition, the fact that the size of sea salts changes with humidity is also
252 considered. The wet deposition of sea salts follows the scheme for soluble aerosols used in
253 CAM4, and depends on prescribed solubility and size-independent scavenging coefficients.

254 **2.4 Dust aerosols**

255 Dust aerosols behave in a similar way as sea salts. Their variations involve three major
256 processes: emission, advective transport, and wet/dry depositions. The dust emission is based
257 on a saltation-sandblasting process, and depends on wind friction velocity, soil moisture, and
258 vegetation/snow cover (Zender et al., 2003). The vertical flux of dust emission is corrected by
259 a surface erodible factor at each model grid cell which has been downloaded from NCAR

260 website (<https://svn-ccsm-inputdata.cgd.ucar.edu/trunk/inputdata/atm/cam/dst/>). Soil
 261 erodibility is prescribed by a physically-based geomorphic index that is proportional to the
 262 runoff area upstream of each source region (Albani et al., 2014). Like sea salts, dry deposition
 263 of dust aerosols includes gravitational and turbulent deposition processes, while wet
 264 deposition results from both convective and large scale precipitation and is dependent on
 265 prescribed size-independent scavenging coefficients.

266 **2.5 Effects of aerosols on radiation, clouds, and precipitation**

267 The mass mixing ratios of bulk aerosols are prognostic variables in BCC-ESM1 and
 268 directly affect the radiative transfer in the atmosphere with their treatments following the
 269 NCAR Community Atmosphere Model (CAM3, Collins et al., 2004). Indirect effects of
 270 aerosols are taken into account in the present version of BCC-AGCM3-Chem (Wu et al.,
 271 2019). Aerosol particles act as cloud condensation nuclei and exert influence on cloud
 272 properties and precipitation, and ultimately impact the hydrological cycle.

273 Prognostic aerosol masses are used to estimate the liquid cloud droplet number
 274 concentration N_{cdnc} (cm^{-3}) in BCC-AGCM3-Chem. N_{cdnc} is explicitly calculated using the
 275 empirical function suggested by Boucher and Lohmann (1995) and Quaas et al. (2006):

$$276 \quad N_{cdnc} = \exp\left[5.1 + 0.41 \ln(m_{aero})\right] \quad (2)$$

277 where m_{aero} ($\mu\text{g}\cdot\text{m}^{-3}$) is the total mass of all hydrophilic aerosols,

$$278 \quad m_{aero} = m_{SS} + m_{OC} + m_{SO_4} + m_{NH_4NO_2}, \quad (3)$$

279 i.e. the first bin of sea salt (m_{SS}), hydrophilic organic carbon (m_{OC}), sulphate (m_{SO_4}), and
 280 [Ammonium nitrite \(\$NH_4NO_2\$ \)](#). A dataset of NH_4NO_2 from NCAR CAM-Chem (Lamarque et
 281 al., 2012) is used in our model.

282 N_{cdnc} is an important factor in determining the effective radius of cloud droplets for
 283 radiative calculation. The effective radius of cloud droplets r_{el} is estimated as

$$284 \quad r_{el} = \beta \cdot r_{l,vol}, \quad (4)$$

285 where β is a parameter dependent on the droplets spectral shape and follows the calculation
 286 proposed by Peng and Lohmann (2003),

$$287 \quad \beta = 0.00084 N_{cdnc} + 1.22. \quad (5)$$

288 $r_{l,vol}$ is the volume-weighted mean cloud droplet radius,

$$289 \quad r_{l,vol} = \left[(3LWC) / (4\pi\rho_w N_{cdnc}) \right]^{1/3}, \quad (6)$$

290 where ρ_w is the liquid water density and LWC the cloud liquid water content (g cm^{-3}).

291 Aerosols also exert impacts on precipitation efficiency (Albrecht, 1989), which is taken
292 into account in the parameterization of non-convective cloud processes. There are five
293 processes that convert condensate to precipitate: auto-conversion of liquid water to rain,
294 collection of cloud water by rain, auto-conversion of ice to snow, collection of ice by snow,
295 and collection of liquid by snow. The auto-conversion of cloud liquid water to rain ($PWAUT$)
296 is dependent on the cloud droplet number concentration and follows a formula that was
297 originally suggested by Chen and Cotton (1987),

$$298 \quad PWAUT = C_{l,aut} q_l^2 \rho_a / \rho_w \left(\frac{q_l \rho_a}{\rho_w N_{ncdc}} \right)^{1/3} H(r_{l,vol} - r_{lc,vol}) \quad (7)$$

299 Where \hat{q}_l is in-cloud liquid water mixing ratio, ρ_a and ρ_w are the local densities of air and
300 water respectively, and $C_{l,aut}$ is a constant. $H(x)$ is the Heaviside step function with the
301 definition,

$$302 \quad H(x) = \begin{cases} 0, & x < 0 \\ 1, & x \geq 0 \end{cases}. \quad (8)$$

303 $r_{lc,vol}$ is the critical value of mean volume radius of liquid cloud droplets $r_{l,vol}$, and set to 15
304 μm .

305 The treatment of aerosol single scattering (optical) properties (such as mass extinction
306 efficiency, single scattering albedo, and asymmetric factor) follows the look-up table
307 approach in CAM (Collins et al., 2004). The optics for black, organic carbon, sea salt, and sea
308 salt particles is assumed to be same as the optics for soot and water-soluble aerosols in the
309 Optical Properties of Aerosols and Clouds (OPAC) data set (Hess et al., 1998). The optics for
310 dust is derived by Mie calculations for the size distribution represented by each size bin
311 (Zender et al., 2003). Similarly, for sulfate and nitrate particles, same set of aerosol optical
312 properties for ammonium sulfate are used and are taken from Wang et al. (2008b) with
313 treatment of aerosol hygroscopicity. The volcanic stratospheric aerosols are assumed to be
314 comprised of 75% sulfuric acid and 25% water, as in Hess et al. (1998). For each model year,

different aerosol types are assumed to be externally mixed in the calculation of bulk aerosol single scattering properties that are in turn used in the radiative transfer calculations.

3. Experiment design for the 20th century climate simulation

There is an Aerosol Chemistry Model Intercomparison Project (AerChemMIP, Collins et al., 2017) endorsed by the Coupled-Model Intercomparison Project 6 (CMIP6) for documenting and understanding past and future changes in the chemical composition of the atmosphere, and estimating the global-to-regional climate response from these changes. Modelling groups with full chemistry and aerosol models are encouraged to perform all AerChemMIP simulations (Collins et al., 2017). To assess the ability of our model to simulate aerosols (mean and variability), we have followed the historical simulation designed by CMIP6 (Eyring et al., 2016) which is named as “historical” experiment in the Earth System Grid Federation (ESGF). ~~The protocol details of the historical experiment is forced with emissions evolving from 1850 to 2014 refer to Collins et al. (2017) that include biomass burning emissions (Van Marle et al. 2017), anthropogenic and open burning emissions (Hoesly et al., 2018; Feng et al., 2019).~~ O₃ in the historical simulation is an interactive prognostic variable and feedbacks on radiation, and the concentrations of other WMOGHG, e.g. CH₄, N₂O, CO₂, CFC11, and CFC12 are prescribed using CMIP6 historical forcing data ~~(Meinshausen et al., 2017) as suggestion in AerChemMIP protocol.~~ Although CH₄ and N₂O are prognostic variables in the chemistry scheme (Table 1), their prognostic values at each model step in the historical experiment are replaced by CMIP6 data (Meinshausen et al., 2017) throughout the model domain. The rest of historical forcing data include: (1) yearly global gridded land-use forcing data sets (Hurtt et al., 2011; Hurtt et al., 2017), and (2) solar forcing (Matthes et al., 2017). All these datasets were downloaded from <https://esgf-node.llnl.gov/search/input4mips/>. Climate feedback processes that involve changes to the atmospheric composition of reactive gases and aerosols may affect the temperature response to a given WMOGHG concentration level ~~(Collins et al., 2017).~~ ~~Three members of historical experiments are conducted and the first member is analyzed in this work.~~

3.1 Surface emissions

Surface emissions of chemical species from different sources are summarized in Table

345 4. They include anthropogenic emissions from fossil fuel burning and other industrial
346 activities, biomass burning (including vegetation fires, fuel wood and agricultural burning),
347 biogenic emissions from vegetation and soils, and oceanic emissions. Most historical
348 emissions from anthropogenic source (surface, aircraft plus ship) and biomass burning from
349 | 1850 to 2014 are CMIP6-recommended data (~~Hoesly et al., 2018;~~ available at
350 <https://esgf-node.llnl.gov/search/input4mips>). Anthropogenic or biomass burning sources of
351 some tracers which are not included in the CMIP6 dataset (see Table 4), anthropogenic
352 emission of H₂ and N₂O are from monthly climatological dataset provided by the MOZART-2
353 standard package. N₂O is a prognostic variable in BCC-ESM1 but it is replaced by CMIP6
354 prescribed concentration in the historical run. Other emissions including biomass burning
355 (CH₃COCH₃) and anthropogenic emission (CH₃CHO, CH₃OH, and CH₃COCH₃) are from the
356 | [IPCC–Atmospheric Chemistry and Climate Model Intercomparison Project \(ACCMIP\)](#)
357 emission inventory (<http://accent.aero.jussieu.fr/ACCMIP.php>) covering the period from 1850
358 to 2010 with 10-year intervals (see Table 4). Monthly lumped emissions of black carbon and
359 organic carbon aerosols from 1850 to 2014 are downloaded from CMIP6-recommended data,
360 but we used 80% (for BC) and 50% (for OC) of them in their hydrophobic forms (BC1 and
361 OC1) and the rest in their hydrophilic forms (BC2 and OC2), following the work of Chin et al.
362 (2002).

363 Five tracers of ISOP, ACET (CH₃COCH₃), C₂H₄, C₃H₈, and Monoterpenes (C₁₀H₁₆) in
364 Table 1 belong to biogenic volatile organic carbons (VOCs). As shown in Table 4, those
365 VOCs emissions are online calculated in BCC-ESM1 following the modeling framework of
366 the Model of Emissions of Gases and Aerosols from Nature version 2.1 (MEGAN2.1,
367 Guenther et al., 2012) using simple mechanistic algorithms to account for major known
368 processes controlling biogenic emissions. The MEGAN2.1 can provide a flexible scheme for
369 estimating 16 tracers of biogenic emissions from terrestrial ecosystems including five VOCs
370 emissions used in BCC-ESM1 (Table 4). All the VOCs emissions depend on current and past
371 surface air temperature, solar flux, and the landscape types. Their calculation requires global
372 maps of plant functional type (PFT) and leaf area index (LAI) which is a prognostic variable
373 from the land model BCC-AVIM2. The effect of atmospheric CO₂ concentration on isoprene
374 emissions is included. 10% of the biogenic monoterpenes emissions as calculated online with

375 the MEGAN2.1 algorithm in BCC-AVIM2 are converted to hydrophilic organic carbon (OC2)
376 to account for formation of secondary organic aerosols following Chin et al. (2002) in this
377 version of BCC-ESM1.

378 **3.2 Volcanic eruptions, lightning and aircraft emissions**

379 As there is no stratospheric aerosol scheme in BCC-ESM1, concentrations of sulfate
380 aerosol at heights from 5 to 39.5 km, which volcanic origin, are directly prescribed using the
381 CMIP6-recommended data (Thomasson et al., 2018) from 1850 to 2014. The effects of
382 surface SO₂ emissions from volcanic eruption on the variation of SO₂ in the atmosphere and
383 then on the variation of tropospheric SO₄²⁻ concentration are considered, and the SO₂
384 emissions from 1850 to 2014 are downloaded from the IPCC ACCMIP emission inventory
385 (<http://accent.aero.jussieu.fr/ACCMIP.php>). Aircraft emissions are provided for NO₂, CO,
386 CH₄, NH₃, NO, SO₂, and aerosols of OC and BC (Table 1). The emissions of NO from
387 lightning are online calculated in BCC-AGCM3-Chem following the parameterization in
388 MOZART2, and the globally-averaged mean during the period of 1850 to 2014 is 5.19
389 Tg(N) yr⁻¹, which is in agreement with observations within the range of 3 to 6 Tg(N) yr⁻¹
390 (Martin et al., 2002). The lightning frequency depends strongly on the convective cloud top
391 height, and the ratio of cloud-to-cloud versus cloud-to-ground lightning depends on the cold
392 cloud thickness from the level of 0°C to the cloud top (Price and Rind, 1992).

393 **3.3 Upper boundary of the atmosphere**

394 As no stratospheric chemistry is included in the present version of BCC-AGCM3-Chem,
395 it is necessary to ensure a proper distribution of chemically-active stratospheric species.
396 Concentrations of different tracers (O₃, CH₄, N₂O, NO, NO₂, HNO₃, CO, and N₂O₅) at the top
397 two layers of the model are set to prescribed monthly climatological values, and
398 concentrations from below the top two layers to the tropopause are relaxed at a relaxation
399 time of 10-days towards the climatology. Climatological values of NO, NO₂, HNO₃, CO and
400 N₂O₅ at the top two layers are extracted from MOZART2 data package available at the
401 Website (<https://www2.acom.ucar.edu/gcm/mozart-4>), originated from the Study of Transport
402 and Chemical Reactions in the Stratosphere (STARS, Brasseur et al., 1997). Concentrations
403 for the other tracers (O₃, CH₄, and N₂O) at the top two model layers are the zonally-averaged
404 and monthly values from 1850 to 2014 derived from the CMIP6 data package.

405 3.4 The preindustrial model states

406 The preindustrial state of BCC-ESM1 is obtained from a piControl simulation of over 600
407 years in which all forcings including emissions data are fixed at 1850 conditions. The initial
408 state of the piControl simulation itself is obtained through individual spin-up runs of each
409 component of BCC-ESM1 in order for the piControl simulation to run stably and fast to reach
410 its equilibrium. Figures 1(a-c) show the time series of global yearly means of the net energy
411 budget at top of the atmosphere (TOA), near-surface air temperature (TAS), and sea surface
412 temperature (SST) from the piControl simulation for the last 450 years. It shows that the
413 surface climate in BCC-ESM1 nearly reaches its equilibrium after 600 years piControl
414 simulation. The whole system in BCC-ESM1 fluctuates around $+0.7 \text{ Wm}^{-2}$ net energy flux at
415 TOA without obvious trend in 450 years (Fig. 1a). This level of TOA energy imbalance is
416 close to the average imbalance (1.0 Wm^{-2}) among CMIP5 models (Wild et al., 2013). It
417 means that there exists surplus energy of $+0.7 \text{ Wm}^{-2}$ obtained by the whole system in
418 BCC-ESM1, but ~~and~~ do not cause remarkable climate drift ~~in BCC-ESM1~~. The global mean
419 TAS and SST keep around 288.1 K (Fig. 1b) and 295.05 K (Fig. 1c), respectively. During the
420 last 450 years, there are ($\pm 0.2 \text{ K}$ amplitude of TAS and SST) oscillations of centennial scale
421 for the whole globe (Figs. 1b and 1c), which are certainly caused by internal variation of the
422 system.

423 Figures 2a-2c show the time series of global annual total burdens of SO_2 , DMS, and OH
424 in the troposphere (integrated from the surface to 100 hPa) in the last 450 years of the
425 piControl simulation. Without any anthropogenic source, the SO_2 amount in the troposphere
426 nearly keeps the level of 0.0868 Tg in the 450 years of the piControl simulation. Tropospheric
427 DMS varies around the value of 0.116 Tg. Tropospheric OH, as an important gas species
428 oxidizing SO_2 to form SO_4^{2-} (Table 2), keeps at a stable level in the atmosphere. SO_4^{2-} also
429 remains at a stable level of 0.556 Tg in the atmosphere in the whole period of the piControl
430 simulation (Figure 2d). The amounts of BC and OC in the troposphere vary around 0.0395 Tg
431 and 0.275 Tg (Figures 2e-2f), respectively. Dust and sea salt aerosols are at the level of 22 Tg
432 and 11.7 Tg (Figures 2g-2h), respectively. All those data are close to the global mean
433 concentrations of 0.604 Tg SO_4^{2-} , 0.046 Tg BC, 0.30 Tg OC, 22.18 Tg dust, and 11.73 Tg sea
434 salts in 1850 which are estimated based on the CMIP5 prescribed data in 1850 (Lamarque et

435 al., 2010).

436 Figure 3 shows the global spatial distributions of annual mean sulfate, organic carbon,
437 black carbon, dust, and sea salt aerosols in the whole atmospheric column averaged for the
438 last 100 years of the piControl simulation of BCC-ESM. We can compare them with CMIP5
439 recommended concentrations in year 1850, considered as the reference state in the
440 pre-industrial stage. At that time, there are fewer anthropogenic/biomass SO_2 emissions, the
441 SO_4^{2-} over land are evidently smaller than those over oceans especially over the tropical
442 Pacific and Atlantic Oceans, where DMS can be oxidized to SO_2 and then form SO_4^{2-} . There
443 are several centers of high values of black carbon and organic carbon in East and South Asia,
444 Europe, Southeast America, and in the tropical rain forests in Africa and South America.
445 They mainly result from biomass burning including vegetation fires, fuel wood and
446 agricultural burning. Dust aerosols are mainly distributed in North Africa, Central Asia, North
447 China, and Australia, where arid and semi-arid areas locate. Dust emitted from Sahara Desert
448 can be transported to the tropical Atlantic by easterly wind. The sea salt aerosols are mainly
449 distributed over the mid-latitude Southern Oceans, the tropical southern Indian Ocean, and the
450 tropical northern Pacific Ocean, where wind speeds near the sea surface are strong. As shown
451 in Fig. 3, all the spatial distribution patterns of CMIP5-derived sulfate, black carbon, organic
452 carbon, dust, and sea salt aerosols (Lamarque et al., 2010) are well simulated in BCC-ESM1.
453 There are high spatial correlation coefficients, 0.76 for sulfate, 0.77 for black carbon, 0.77 for
454 organic carbon, 0.94 for dust, and 0.94 for sea salts, between CMIP5 data and BCC-ESM1
455 simulations. Relative lower relations for sulfate, black carbon and organic carbon are possibly
456 caused as different anthropogenic emission sources are used in BCC-ESM1 and to create
457 CMIP5 data. Dust and sea salts belong to natural aerosols and depend on the land and sea
458 surface conditions, so their spatial distributions are easy to be captured and have relatively
459 higher correlations between CMIP5 data and BCC-ESM1 simulations.

460

461 **4. Evaluation of O_3 and aerosol simulations in the 20th century**

462 The rate of sulfate formation is dependent on the levels of oxidants in the troposphere.
463 O_3 is an important oxidant. So, the evaluation of simulated tropospheric O_3 is helpful to
464 understand the aerosols simulations. BCC-ESM1 is driven by most of the

465 CMIP6-recommended emission data. As shown in Figure 4, the zonal distributions of the total
466 amounts of tropospheric O₃ below 300 hPa to the ground and their changes with time from
467 1850 to 2014 from the CMIP6-recommend dataset (Table 4) are well simulated by
468 BCC-ESM1. Evident increasing trends since 1850 almost exist in every latitudes, especially
469 in the Northern Hemisphere where the contents of tropospheric O₃ are higher than those in the
470 Southern Hemisphere.

471 Figure 5 shows the vertical profiles of O₃ simulations with comparison to global
472 ozonesonde observations averaged for the monthly data over 2010-2014 from the World
473 Ozone and Ultraviolet Radiation Data Centre (WOUDC; <http://woudc.org/data.php>, last
474 access: 24 September 2019) in nine regions which are averaged from 41 global WOUDC sites.
475 The details of WOUDC data may refer to Lu et al. (2019). As shown in Figure 5, BCC-ESM1
476 well captures the observed ozone vertical structure at all regions. At the lower and middle
477 troposphere (i.e. below 6 km), the model typically shows positive bias within 5 ppbv for the
478 Southern Hemisphere and 10 ppbv for the Northern mid-latitudes, similar to those simulated
479 from many other global atmospheric chemical models (Young et al., 2013, 2018). The model
480 has larger ozone overestimation in the upper troposphere and stratosphere at most regions, at
481 least partly due to the use of prescribed stratospheric ozone as upper boundary conditions
482 and/or errors in modeling ozone exchange between the stratosphere and the troposphere.
483 Global tropospheric ozone burden derived from our simulation is 335 Tg averaged over
484 2010-2014, in consistent with recent assessment from multi chemistry models (Young et al.,
485 2018).

486 **4.1 Global aerosols trends**

487 Figure 6(a)-(c) show the time series of global total emissions of SO₂, OC, and BC to the
488 atmosphere from natural and anthropogenic sources. Emissions of SO₂ are largely due to
489 industrial production. From 1850 to 1915, SO₂ emissions increased year by year as the
490 Industrial Revolution intensified and expanded. But from 1915 to 1945, the increase trend of
491 SO₂ emissions became slower as broke out the First and the Second World Wars. After that
492 period, with growing industrial productions, SO₂ emissions increased again and reached a
493 maximum around the end of 1970s. During the 1980s and 2000s, with a substantial decrease
494 of SO₂ emissions in Europe and the United States, the global SO₂ emissions has been

495 decreasing since the 1980s despite the rapid increase of SO₂ emissions in South and East Asia
496 as well as in developing countries in the Southern Hemisphere in recent years (Liu et al.,
497 2009). The OC and BC emissions substantially increased since 1950s just after the Second
498 World War. The global total OC emission in 2010 was nearly twice as much as that in
499 pre-industrial (year 1850) and increased by 18 Tg • yr⁻¹. Anthropogenic black carbon
500 emissions increased from 1 Tg yr⁻¹ in 1850 to nearly 8 Tg yr⁻¹ in 2010.

501 Anthropogenic SO₂, OC and BC emissions strongly affect the variations of atmospheric
502 concentrations of sulfate, OC, and BC. The global 0.5°x0.5° gridded data of
503 CMIP5-recommended aerosols masses with 10-years interval from 1850 to 2000 (Lamarque
504 et al., 2010) provides an important reference to evaluate the aerosol simulations in
505 BCC-ESM1. As shown in Figure 7b-7f, the annual total aerosol burdens of SO₄²⁻, OC, and BC
506 in the whole atmosphere column as simulated by the BCC-ESM1 20th century historical
507 simulation are generally consistent with the values derived from CMIP5-recommended
508 aerosols concentrations. Due to increasing SO₂ emissions from 1850 to present day (Fig. 6),
509 the global SO₂ burden in the atmosphere increased from 100 Tg in 1850s to 200 Tg in 1980s
510 (Fig. 7a), and has a high correlation coefficient of 0.996 with the anthropogenic emissions
511 (Fig. 6a), as the lifetime of SO₂ is short. The burden directly followed the emission. DMS in
512 the atmosphere is oxidized by OH and NO₃ to form SO₂ (Table 2). Its natural emissions from
513 oceans from 1850 to 2010 in the model are the climatological monthly means (Dentener et al.,
514 2006) from MOZART2 data package. As shown in Fig 7a, the global amount of DMS in the
515 whole atmosphere was about 0.12 Tg during 1850-1900 and decreased to 0.055 Tg in 2010.
516 This decrease trend maybe partly results from the speeded rate of DMS oxidation with global
517 warming, and the loss of DMS gradually exceeds the source of ocean DMS emission to cause
518 a net loss of DMS in the atmosphere since 1910s. Largely driven by SO₂ anthropogenic
519 emissions, the sulfate burden shows three different stages from 1850 to present. In the first
520 period from 1850s to 1900s, the sulfate burden had a weak linear increase. It increased
521 significantly in the second stage from 1910's to 1940's, and then exploded since 1950's, until
522 the middle 1970s and early 1980s. The sulfate burden then remained nearly stable and even
523 showed slightly decreases as seen from the CMIP5 data. As for global BC and OC burdens,
524 BCC-ESM1 results show continuous increases since 1850s, especially from 1950 to present.

525 From 1910's to 1940's, the CMIP5 data show a slight decrease of BC and OC burdens in the
526 atmosphere.

527 The dust and sea salt aerosols in the atmosphere are largely determined by the
528 atmospheric circulations and states of the land and ocean surface. We can see that the global
529 dust burden in the atmosphere showed evident increase from 1980 to 2000, which could be
530 partly caused by evident global warming since 1980 and increasing soil dryness resulting in
531 more surface dust to be released in the atmosphere. Their details will be explored in the other
532 paper.

533 **4.2 Global aerosols budgets**

534 We further evaluate global aerosols budgets by comparing a 10-year average of
535 BCC-ESM results from 1990 to 2000 with various studies for sulfate, BC, OC, sea salt, and
536 dust. Their annual total emissions, average atmospheric mass loading, and mean lifetimes are
537 listed in Tables 5 and 6. It is worth emphasizing that the global mean total source and sink for
538 each type of aerosols in BCC-ESM1 are almost balanced.

539 The global DMS emission from the ocean is $27.4 \text{ Tg(S) yr}^{-1}$ in BCC-ESM. This
540 emission in BCC-ESM is nearly balanced by the gas-phase oxidation of DMS to form SO_2 .
541 The DMS burden is 0.12 Tg with a lifetime of 0.78 days, which is within the range of other
542 models reported in the literature. As shown in Table 5, the total SO_2 production averaged for
543 the period of 1991 to 2000 is $76.93 \text{ Tg(S) yr}^{-1}$. A rate of $13.2 \text{ Tg(S) yr}^{-1}$ (about 17%) SO_2 is
544 produced from the DMS oxidation, only $0.1 \text{ Tg(S) yr}^{-1}$ SO_2 from airplane emissions to the
545 atmosphere, and the rest ($63.63 \text{ Tg(S) yr}^{-1}$, near 82.7%) from anthropogenic activities and
546 volcanic eruption at surface. The amount of SO_2 produced from the DMS oxidation is in the
547 range of other works (10.0 to $24.7 \text{ Tg(S) yr}^{-1}$) reported in Liu et al (2005). All the SO_2
548 production is balanced by SO_2 losses by dry and wet deposition, and by gas- and
549 aqueous-phase oxidation. Half of its loss ($38.74 \text{ Tg(S) yr}^{-1}$) occurs via its aqueous-phase
550 oxidation to form sulfate. Other losses through dry and wet depositions and gas-phase
551 oxidation to form SO_4^{2-} are also important (Table 2). All the sinks are in the range from the
552 literature (Liu et al., 2005). The global burden of SO_2 in the atmosphere is 0.48 Tg with a
553 lifetime of 1.12 days, consistent with values in literature (Liu et al., 2005).

554 Sulfate aerosol is mainly produced from aqueous-phase SO_2 oxidation ($38.73 \text{ Tg(S) yr}^{-1}$)

555 and partly from gaseous phase oxidation of SO_2 ($10.32 \text{ Tg(S) yr}^{-1}$), and is largely lost by wet
556 scavenging ($49.06 \text{ Tg(S) yr}^{-1}$). The total SO_4^{2-} production in BCC-ESM is at the lower range
557 of values in other models reported in Textor et al. (2006). Its global burden is 1.89 Tg and the
558 lifetime is 4.69 days, which are within the range of 1.71 to 2.43 Tg and 3.3 to 5.4 days in the
559 literatures (Textor et al., 2006; Liu et al., 2012; Liu et al., 2016; Matsui and Mahowald, 2017;
560 Tegen et al., 2019; the value derived from CMIP5 data).

561 Sources of BC and OC are mainly from anthropogenic emissions. Based on the CMIP6
562 data, there are, on average, 7.22 Tg yr^{-1} BC and 13.91 Tg yr^{-1} OC from fossil and bio-fuel
563 emissions and 18.38 Tg yr^{-1} OC from natural emission during the period of 1991 to 2000.
564 Most of them are scavenged through convective and large-scale rainfall processes. The rest
565 returns to the surface by dry deposition. The simulated global BC and OC burdens are 0.13
566 and 0.62 Tg, respectively (Table 6), all close to values of 0.114 Tg BC and 0.69 Tg OC
567 derived from the CMIP5 data, and within the range of 0.11-0.26 Tg BC (Textor et al., 2006;
568 Matsui and Mahowald, 2017; Tegen et al., 2019) and less than the values of 1.25-2.2 Tg OC
569 in other literatures (Textor et al., 2006; Tegen et al., 2019). The simulated BC and OC
570 lifetimes are 6.6 and 5.0 days respectively, and are close to the recent values of 5.0-7.5 days
571 BC and 5.4-6.6 days OC in literatures (Matsui and Mahowald, 2017; Tegen et al., 2019).

572 The emissions of dust and sea salt are mainly determined by winds near the surface. The
573 annual total dust emission in BCC-ESM1 is 2592 Tg yr^{-1} , higher than AeroCom multi-model
574 mean (1840 Tg yr^{-1} , Textor et al., 2006), but comparable to other studies (Chin et al., 2002;
575 Liu et al., 2012; Matsui and Mahowald, 2017). The average dust loading is 22.93 Tg, lower
576 than the value of 35.9 Tg in Ginoux et al. (2001) but slightly higher than the value of 20.41
577 Tg derived from CMIP5 data. The average lifetime for dust particles is 3.23 days that is
578 shorter than the AeroCom mean (4.14 days) and the value of 3.9 days in recent study (Matsui
579 and Mahowald, 2017). The simulated sea salt emission is $4667.2 \text{ Tg yr}^{-1}$, slightly lower than
580 the simulated value in Liu et al. (2012), and substantially lower than the AeroCom mean
581 (16600 Tg yr^{-1} , Textor et al., 2006). The simulated sea salt burdens are 11.89 Tg and close to
582 the CMIP5 data. Their averaged lifetimes are 0.93 days and close to the value in the recent of
583 Matsui and Mahowald (2017) but longer than the AeroCom mean (0.41days, Textor et al.,
584 2006).

585 **4.3 Global aerosol distributions at present day**

586 Figures 8-12 show December-January-February (DJF) and June-July-August (JJA) mean
587 column mass concentrations of sulfate (SO_4^{2-}), OC, BC, Dust, and Sea Salt aerosols averaged
588 for the period of 1991-2000, respectively. Here, BCC-ESM1 simulated results are compared
589 with the CMIP5-recommended data for the same period. Unlike the pre-industrial level of
590 sulfate shown in Fig. 2, sulfate concentrations at present day (Fig. 8) are strongly influenced
591 by anthropogenic emissions, and have maximum concentrations in the industrial regions (e.g.,
592 East Asia, Europe, and North America). Their seasonal variations are distinct and are
593 characterized by high concentrations in boreal summer and low concentrations in boreal
594 winter. These spatial distributions simulated by BCC-ESM1 are well consistent with the
595 CMIP5 data, with spatial correlation coefficients in DJF and JJA reaching 0.92 and 0.83
596 (Figure 13), respectively. The deviation of the spatial pattern in BCC-ESM1 is less from the
597 CMIP5 data in DJF but larger in JJA (Figure 13).

598 Unlike sulfate whose maximum concentrations are mainly distributed between 60°N
599 and the equator, peaking concentrations of BC and OC as shown in Figs. 9 and 10 are located
600 near the tropics in the biomass burning regions (e.g., the maritime continent, Central Africa,
601 South America), and their seasonal variations from DJF to JJA are evidently weaker than
602 those of sulfate except in South America. In boreal summer, there are centers of high values
603 in the industrial regions in the Northern Hemisphere mid-latitudes (i.e., East Asia, South Asia,
604 Europe, and North America). These main features of spatial and seasonal variations in CMIP5
605 data are well captured by BCC-ESM1, and the BCC-ESM1 vs. CMIP5 spatial correlation
606 coefficients (Figure 13) are 0.90 (OC in DJF), 0.91 (BC in DJF), 0.91 (OC in JJA) and 0.92
607 (BC in JJA). There are less deviations of spatial pattern for OC in DJF and JJA, but larger
608 deviation for BC from CMIP5 data (Figure 13).

609 As show in Figure 11, dust concentrations in the atmosphere show largest values over
610 strong source regions such as Northern Africa, Southwest and Central Asia, and Australia,
611 and over their outflow regions such as the Atlantic and the western Pacific. In DJF, the
612 CMIP5 data shows centers of high concentrations over East Asia and Central North America,
613 but both centers are missing in BCC-ESM1. However, these two high-value centers in the
614 CMIP5 data may not be true, since frozen soils in these areas in winter lead to unfavorable

615 conditions for soil erosion by winds. The spatial correlation coefficients between CMIP5 and
616 BCC-ESM1 remain high: 0.95 in JJA and 0.88 in DJF (Figure 13). Small deviations of spatial
617 pattern for dust simulations in BCC-ESM1 show less magnitude of dust maximums against
618 with CMIP5 data (Figure 13).

619 As shown in Figure 12, high sea salt concentrations are generally over the storm track
620 regions over the oceans, e.g., mid-latitudes in the Northern Oceans in DJF and the Southern
621 Ocean in JJA where wind speeds and thus sea salt emissions are higher. In addition, there is a
622 belt of high sea salt concentrations in the subtropics of both hemispheres where precipitation
623 scavenging is weak. Their spatial distributions in BCC-ESM1 are consistent with the CMIP5
624 data with correlation coefficients of 0.92 in JJA and 0.90 in DJF (Figure 13). The spatial
625 deviations of sea salt are much closer to CMIP5 data than those of sulfate, OC, BC, and dust
626 distributions (Figure 13).

627 Figure 14 shows vertical distributions of zonally-averaged annual mean concentrations
628 of sulfate, organic carbon, black carbon, dust, and sea salt aerosols in the period of 1991-2000.
629 Both BCC-ESM1 and CMIP5 results show that strong sulfur, OC, and BC emissions in the
630 industrial regions of the Northern Hemisphere mid-latitudes can rise upward and be
631 transported towards the North Pole in the mid- to upper troposphere. Most of OC, BC, and
632 dust aerosols are confined below 500 hPa, while sulfate can be transported to higher altitudes.
633 Sea salt aerosols are mostly confined below 700 hPa, as the particles are large in size and
634 favorable for wet removal and gravitational settling towards the surface. It can be seen that
635 BCC-ESM1 tends to simulate less upward transport of aerosols than the CMIP5 data, likely
636 reflecting the omission of deep convection transport of tracers in BCC-ESM1.

637 The CMIP5 data used here are mainly from model simulations. We will further evaluate
638 the BCC-ESM1 model results with ground observations. Annual mean SO_4^{2-} , BC and OC
639 aerosol observations from the Interagency Monitoring of Protected Visual Environments
640 (IMPROVE) sites over 1990-2005 in the United States
641 (<http://vista.cira.colostate.edu/IMPROVE/>) and from the European Monitoring and Evaluation
642 Programme (EMEP) (<http://www.emep.int>) sites over 1995-2005 are used. As shown in
643 Figure 15a and 15b, the BCC-ESM simulated sulfate concentrations are in general
644 comparable to the EMEP observations in Europe, but are systematically by about $1 \mu\text{g m}^{-3}$

645 higher than the U.S. IMPROVE observations. As for BC, there are large model biases at both
646 European and U.S. sites (Figs. 15c and 15d), especially BCC-ESM overestimates BC
647 concentrations at the IMPROVE sites. The observed OC concentrations are slightly
648 overestimated for IMPROVE sites but systematically underestimated for EMEP sites. Some
649 statistical features for simulated concentrations versus EMEP and IMPROVE observations are
650 listed in Table 7. These comparisons are overall fairly reasonable considering the
651 uncertainties in emissions and the coarse model resolution.

652 We then evaluate the simulated BC concentrations from BCC-ESM1 with the HIAPER
653 (High-Performance Instrumented Airborne Platform for Environmental Research)
654 Pole-to-Pole Observations (HIPPO) (Wofsy et al., 2011). The HIPPO campaign provided
655 observations of black carbon concentration profiles over Pacific Ocean and North America
656 between 2009 and 2011. Following Tilmes et al. (2016), model results here are sampled along
657 the HIPPO flight tracks and then averaged to different latitude and altitude bands for
658 comparison. As shown in Figure 16, BCC-ESM1 and HIPPO aircraft observations shows
659 reasonable agreement in terms of the spatial distributions and seasonal variations of BC levels.
660 BCC-ESM1 generally reproduces the observed hemispheric gradients of BC, i.e. the larger
661 burden in the NH compared to the SH, in consistent with Figures 10 and 14. The mean value
662 of modelled results along the flight track is 11.1 ng/kg, comparable to 8.2 ng/kg of the HIPPO
663 observations. The model shows large overestimations of BC observations over the tropics,
664 which is also found in the CAM4-chem global chemical model (Tilmes et al., 2016).

665 **4.4 Aerosol Optical Properties**

666 Aerosol optical depth (AOD) is an indicator of the reduction in incoming solar
667 radiation (at a particular wavelength) due to scattering and absorption of sunlight by aerosols.
668 In this study, we calculate the AOD at 550 nm for all aerosols including sulfate, BC, organic
669 carbon, sea salt and dust as the product of aerosol dry mass concentrations, aerosol water
670 content, and their specific extinction coefficients. The total AOD is calculated by summing
671 the AOD in each model layer for each aerosol species using the assumption that they are
672 externally mixed. The AOD observations retrieved from MODIS and MISR over the period of
673 1997-2003, and from AERONET over the period of 1998–2005 (<http://aeronet.gsfc.nasa.gov>)

674 are used to evaluate the averaged AOD at 550 nm in BCC-ESM. Figure 17 shows averages of
675 MISR and MODIS AOD with corresponding averages from BCC-ESM. The BCC-ESM1
676 simulated AOD generally captures the spatial distribution of MISR and MODIS retrievals.
677 The model overestimates AOD over East China. It also systematically underestimates the
678 MODIS observations in the Southern Hemisphere, but is closer to MISR observations. Figure
679 18 shows multi-years annual means of BCC-ESM1 simulated AOD values versus
680 observations from AERONET over the period of 1998–2005. The basic pattern of modeled
681 global AOD is similar to that of observations and their spatial correlation reaches 0.56. Large
682 values of AOD are mainly distributed in land continents such as North African, South Asia,
683 East Asia, Europe, and eastern part of North America. Figures 19a-19d present scatter plots of
684 observed versus simulated multi-year monthly mean AOD at those sites of AERONET in
685 Europe, North America, East Asia, and South Asia over the period of 1998-2005, respectively.
686 Model simulated monthly AOD generally agrees with observations within a factor of 2 for
687 most sites. BCC-ESM slightly overestimates the AOD in European and North American sites.
688 In those regions, BCC-ESM also slightly overestimates MODIS and MISR AOD observations
689 (Fig. 17).

690 **5. Summary and discussions**

691 This paper presents a primary evaluation of aerosols simulated in version 1 of the Beijing
692 Climate Center Earth System Model (BCC-ESM1) with the implementation of the interactive
693 atmospheric chemistry and aerosol based on the newly developed BCC-CSM2. Global
694 aerosols (including sulfate, organic carbon, black carbon, dust and sea salt) and major
695 greenhouse gases (e.g., O₃, CH₄, N₂O) in the atmosphere can be interactively simulated when
696 anthropogenic emissions are provided to the model. Concentrations of all aerosols in
697 BCC-ESM1 are determined by the processes of advective transport, emission, gas-phase
698 chemical reactions, dry deposition, gravitational settling, and wet scavenging by clouds and
699 precipitation. The nucleation and coagulation of aerosols are ignored in the present version of
700 BCC-ESM1. Effects of aerosols on radiation, cloud, and precipitation are fully included.

701 We evaluate the performance of BCC-ESM1 in simulating aerosols and their optical
702 properties in the 20th century following CMIP6 historical simulation according to the
703 requirement of the AerChemMIP. It is forced with anthropogenic emissions evolving from

704 1850 to 2014 but some WMGHGs such as CH₄, N₂O, CO₂, CFC11 and CFC12 are prescribed
705 using CMIP6 prescribed concentrations (to replace prognostic values of CH₄ and N₂O from
706 the chemistry scheme). Both direct and indirect effects of aerosols are considered in
707 BCC-ESM1. Initial conditions of the CMIP6 historical simulation are obtained from a
708 600-year piControl simulation in the absence of anthropogenic emissions, which well captures
709 the pre-industrial concentrations of SO₄²⁻, organic carbon (OC), black carbon (BC), dust, and
710 sea salt aerosols and are consistent with the CMIP5 recommended concentrations for the year
711 1850. With the CMIP6 anthropogenic emissions of SO₂, OC, and BC from 1850 to 2014 and
712 their natural emissions implemented in BCC-ESM1, the model simulated SO₄²⁻, BC, and OC
713 aerosols in the atmosphere are highly correlated with the CMIP5-recommended data. The
714 long-term trends of CMIP5 aerosols from 1850 to 2000 are also well simulated by
715 BCC-ESM1. Global budgets of aerosols were evaluated through comparisons of BCC-ESM1
716 results for 1990-2000 with reports in various literatures for sulfate, BC, OC, sea salt, and dust.
717 Their annual total emissions, atmospheric mass loading, and mean lifetimes are all within the
718 range of values reported in relevant literature. Evaluations of the spatial and vertical
719 distributions of BCC-ESM1 simulated present-day SO₄²⁻, OC, BC, Dust, and sea salt aerosol
720 concentrations against the CMIP5 datasets and in-situ measurements of surface networks
721 (IMPROVE in the U.S. and EMEP in Europe), and HIPPO aircraft observations indicate good
722 agreement among them. The BCC-ESM1 simulates weaker upward transport of aerosols from
723 the surface to the middle and upper troposphere (with reference to CMIP5-recommended
724 data), likely reflecting a lack of deep convection transport of chemical species in the present
725 version of BCC-ESM1. The AOD at 550 nm for all aerosols including sulfate, BC, OC, sea
726 salt, and dust aerosols was further compared with the satellite AOD observations retrieved
727 from MODIS and MISR and surface AOD observations from AERONET. The BCC-ESM1
728 model results are overall in good agreement with these observations within a factor of 2. All
729 these comparisons demonstrate the success of the implementation of interactive aerosol and
730 atmospheric chemistry in BCC-ESM1.

731 This work has only evaluated the ability of BCC-ESM1 to simulate aerosols. The
732 variations of aerosols especially for sulfate are related to other gaseous tracers such as OH
733 and NO₃ (Table 2), which are determined by the MOZART2 gaseous chemical scheme as

734 implemented in BCC-ESM1, and require further evaluation. As limited length of the text, the
735 other optical feature of aerosols such as extinction coefficients, single scattering albedo and
736 asymmetry parameters, and even their feedbacks on radiation and global temperature change
737 will be explored in the other paper. O₃ is evaluated in this work. Other GHGs such as CH₄ and
738 N₂O concentrations can be simulated when forced with emissions and their simulations also
739 need to be evaluated in future.

740 **6. Code and data availability**

741 The source codes of BCC-ESM1 model are available for use under licence agreement.
742 Readers interested in BCC-ESM1 codes and the model input files required to reproduce the
743 simulations may contact Dr. Tongwen Wu (twwu@cma.gov.cn) for further details.~~Source~~
744 ~~codes of BCC-ESM1 model are freely available upon request addressed to Tongwen Wu~~
745 ~~(twwu@cma.gov.cn).~~ Model output of BCC CMIP6 AerChemMIP simulations described in
746 this paper refer to Zhang et al. (2019) and is distributed through ESGF and freely accessible
747 through the ESGF data portals after registration. Details about ESGF are presented on the
748 CMIP Panel website at <http://www.wcrp-climate.org/index.php/wgcm-cmip/about-cmip>.

749

750 **Author contributions**

751 Tongwen Wu led the BCC-ESM1 development. All other co-authors have contributions
752 to it. Fang Zhang and Jie Zhang designed the experiments and carried them out. Tongwen Wu,
753 Laurent Li, Lin Zhang, Xiaohong Liu, Aixue Hu, and Jun Wang wrote the final document
754 with contributions from all other authors.

755

756 **Acknowledgements**

757 This work was supported by The National Key Research and Development Program of China
758 (2016YFA0602100). All the figures are created by the NCAR Command Language (Version
759 6.6.2) [Software].

760

761 **References**

762 Albani, S., Mahowald, N. M., Perry, A. T., Scanza, R. A., Zender, C. S., Heavens, N. G.,
763 Maggi, V., Kok, J. F., and Otto-Bliesner, B. L.: Improved dust representation in the

764 Community Atmosphere Model, *J. Adv. Model. Earth Syst.*, 6, 541–570,
765 doi:10.1002/2013MS000279, 2014.

766 Albrecht, B.: Aerosols, cloud microphysics, and fractional cloudiness, *Science*, 245, 1227–
767 1230, 1989.

768 Arora, V., Boer, G., Friedlingstein, P., Eby, M., Jones, C., Christian, J., Bonan, G., Bopp, L.,
769 Brovkin, V., Cadule, P., Hajima, T., Ilyina, T., Lindsay, K., Tjiputra, J., and Wu, T.:
770 Carbon-concentration and carbon-climate feedbacks in CMIP5 Earth system models. *J.*
771 *Climate*, 26, 5289–5314, 2013.

772 Austin, J., Butchart, N., and Shine, K. P.: Possibility of an Arctic ozone hole in a
773 doubled-CO₂ climate, *Nature*, 360, 221–225, 1992

774 Barth, M.C., Rasch, P.J., Kiehl, J.T., Benkowitz, C.M., and Schwartz, S.E.: Sulfur chemistry
775 in the National Center for Atmospheric Research Community Climate Model:
776 Description, evaluation, features, and sensitivity to aqueous chemistry. *J. Geophys. Res.*,
777 105, D1, 1387-1415, 2000.

778 Bey I., Jacob, D. J., Yantosca, R. M., Logan, J. A., Field, B., Fiore, A. M., Li, Q., Liu, H.,
779 Mickley, L. J., and Schultz, M.: Global modeling of tropospheric chemistry with
780 assimilated meteorology: Model description and evaluation, *J. Geophys. Res.*, 106,
781 23,073-23,096, 2001

782 Boucher, O., Lohmann, U.: The sulphate-CCN-cloud albedo effect – a sensitivity study with
783 two general circulation models, *Tellus* 47B, 281–300, 1995.

784 Brasseur, G. P., Hauglustaine, D. A., Walters, S., Rasch, P. J., Müller, J.-F., Granier, C., and
785 Tie, X. X.: MOZART, a global chemical transport model for ozone and related chemical
786 tracers: 1. Model description, *J. Geophys. Res.*, 103, 28,265– 28,289, 1998.

787 Brasseur, G. P., Tie, X. X., Rasch, P. J., and Lefèvre, F.: A three - dimensional simulation of
788 the Antarctic ozone hole: Impact of anthropogenic chlorine on the lower stratosphere and
789 upper troposphere, *J. Geophys. Res.*, 102, 8909–8930, 1997.

790 Cariolle, D., Lasserre-Bigorry, A., and Royer, J.-F.: A general circulation model simulation of
791 the springtime Antarctic ozone decrease and its impact on midlatitudes, *J. Geophys. Res.*,
792 95, 1883–1898, 1990.

793 [Cess, R. D.: Nuclear war: Illustrative effects of atmospheric smoke and dust upon solar](#)
794 [radiation, *Clim. Change*, 7, 237–251, 1985.](#)

795 Chen, C., and Cotton, W. R.: The physics of the marine stratocumulus-capped mixed layer, *J.*

796 Atmos. Sci., 44 (50), 2951–2977, 1987.

797 Chin, M., Ginoux, P., Kinne, S., Torres, O., Holben, B.N., Duncan, B.N., Martin, R.V., Logan, J.A.,
798 Higurashi, A., Naka-jima, T.: Tropospheric aerosol optical thickness from the GOCART
799 model and comparisons with satellite and Sun photometer measurements. *J. Atmos.*
800 *Sci.* 59:461–483, 2002.

801 Chuang, C. C., Penner, J. E., Taylor, K. E., Grossman, A. S., and Walton, J. J.: An assessment
802 of the radiative effects of anthropogenic sulfate, *J. Geophys. Res.*, 102, 3761–3778,
803 1997.

804 Collins, W. J., Lamarque, J.-F., Schulz, M., Boucher, O., Eyring, V., Hegglin, M. I.,
805 Maycock, A., Myhre, G., Prather, M., Shindell, D., Smith, S. J.: AerChemMIP:
806 quantifying the effects of chemistry and aerosols in CMIP6, *Geosci. Model Dev.*, 10,
807 585–607, 2017.

808 Collins, W. D., Rasch, P. J., Boville, B. A., Hack, J. J., McCaa, J. R., Williamson, D. L.,
809 Kiehl, J. T., Briegleb, B. P., Bitz, C., Lin, S.-J., Zhang, M., and Dai, Y.: Description of
810 the NCAR Community Atmosphere Model (CAM3). *Nat. Cent. for Atmos. Res.*,
811 Boulder, Colo., 2004.

812 Cooke, W.F., Wilson, J.J.N.: A global black carbon aerosol model. *J. Geophys. Res. Atmos.*
813 101, 19395–19409, 1996.

814 Cunnold, D., Alyea, F., Phillips, N., Prinn, R.: A three-dimensional dynamical-chemical
815 model of atmospheric ozone, *J. Atmos. Sci.*, 32, 170-194, 1975.

816 Dentener, F., Kinne, S., Bond, T., Boucher, O., Cofala, J., Generoso, S., Ginoux, P., Gong, S.,
817 Hoelzemann, J. J., Ito, A., Marelli, L., Penner, J. E., Putaud, J.-P., Textor, C., Schulz, M.,
818 van der Werf, G. R., and Wilson, J.: Emissions of primary aerosol and precursor gases in
819 the years 2000 and 1750 prescribed data-sets for AeroCom, *Atmos. Chem. Phys.*, 6,
820 4321–4344, doi:10.5194/acp-6-4321-2006, 2006.

821 Eyring, V., Bony, S., Meehl, G. A., Senior, C. A., Stevens, B., Stouffer, R. J., and Taylor, K.
822 E.: Overview of the Coupled Model Intercomparison Project Phase 6 (CMIP6)
823 experimental design and organization, *Geosci. Model Dev.*, 9, 1937–1958,
824 doi:10.5194/gmd-9-1937-2016, 2016.

825 Feichter, J., Kjellstrom, E., Rodhe, H., Dentener, F., Lelieveld, J., Roelofs, G.-J.: Simulation
826 of the tropospheric sulfur cycle in a global climate model, 30: 1693-1707, 1996.

827 [Feng, L., Smith, S. J., Braun, C., Crippa, M., Gidden, M. J., Hoesly, R., Klimont, Z., van](#)

828 [Marle, M., van den Berg, M., and van der Werf, G. R.: Gridded Emissions for CMIP6,](#)
829 [Geosci. Model Dev. Discuss., <https://doi.org/10.5194/gmd-2019-195>, 2019](#)

830 Ghan, S. J. and Easter, R. C.: Impact of cloud-borne aerosol representation on aerosol direct
831 and indirect effects, *Atmos. Chem. Phys.*, 6, 4163–4174, 2006.

832 Ginoux, P., M. Chin, I. Tegen, J. M. Prospero, B. Holben, O. Dubovik, and S.-J. Lin (2001),
833 Sources and distributions of dust aerosols simulated with the GOCART model, *J.*
834 *Geophys. Res.*, 106, 20,255 – 20,274.

835 Giorgi, F., and Chameides, W. L.: The rainout parameterization in a photochemical model, *J.*
836 *Geophys. Res.*, 90, 7872–7880, 1985.

837 Guenther, A. B., Jiang, X., Heald, C. L., et al.: The Model of Emissions of Gases and
838 Aerosols from Nature Version 2.1 (MEGAN2.1): An Extended and Updated Framework
839 for Modeling Biogenic Emissions. *Geoscientific Model Development* 5(6): 1471–1492,
840 2012.

841 Guenther, A., Baugh, B. Brasseur, G., Greenberg, J., Harley, P., Klinger, L., Serca, D., and
842 Vierling, L.: Isoprene emission estimates and uncertainties for the Central African
843 EXPRESSO study domain, *J. Geophys. Res.*, 104(D23), 30,625–630,639, 1999.

844 [Hess, M., Koepke, P., Schult, I.: Optical properties of aerosols and clouds: the software](#)
845 [package OPAC, *Bull. Am. Meteorol. Soc.*, 79, 831–844, 1998.](#)

846 Hoesly, R. M., Smith, S. ., Feng, L., Klimont, Z., Janssens-Maenhout, G., Pitkanen, T.,
847 Seibert, J. J., Vu, L., Andres, R. J., Bolt, R. M., Bond, T. C., Dawidowski, L., Kholod, N.,
848 Kurokawa, J., Li, M., Liu, L., Lu, Z., Moura, M. C. P., O’Rourke, R. R., and Zhang Q.:
849 Historical (1750–2014) anthropogenic emissions of reactive gases and aerosols from the
850 Community Emission Data System (CEDS), *Geosci. Model Dev.*, 11, 369-408, 2018

851 Horowitz, L.W., Walters, S., Mauzerall, D. L., Emmons, L. K., Rasch, P. J., Granier, C., Tie,
852 X., Lamarque, J.-F., Schultz, M. G., Tyndall, G. S., Orlando, J. J., Brasseur, G. P.: A
853 global simulation of tropospheric ozone and related tracers: Description and evaluation
854 of MOZART, version 2, *J. Geophys. Res.*, 108(D24), 4784, doi:10.1029/2002JD002853,
855 2003.

856 Horowitz, L. W.: Past, present, and future concentrations of tropospheric ozone and aerosols:
857 Methodology, ozone evaluation, and sensitivity to aerosol wet removal, *J. Geophys. Res.*,
858 111, D22211, doi:10.1029/2005JD006937, 2006.

859 Hoffman, F. M., Randerson, J. T., Arora, V. K., Bao, Q., Cadule, P., Ji, D., Jones, C. D.,

860 Kawamiya, M., Khatiwala, S., Lindsay, K., Obata, A., Shevliakova, E., Six, K. D.,
861 Tjiputra, J. F., Volodin, E. M., and Wu, T.: Causes and implications of persistent
862 atmospheric carbon dioxide biases in Earth System Models, *J. Geophys. Res. Biogeosci.*,
863 119, 141–162, doi:10.1002/2013JG002381, 2014.

864 Holtslag, A. A. M., and Boville, B. A.: Local versus nonlocal boundary-layer diffusion in a
865 global climate model, *J. Climate*, 6, 1825–1842, 1993.

866 Hurt, G.C., Chini, L.P., Froking, S. et al.: Harmonization of land-use scenarios for the period
867 1500–2100: 600 years of global gridded annual land-use transitions, wood harvest, and
868 resulting secondary lands, *Climatic Change*, 109, 117-161, 2011.

869 Hurt, G., et al.: input4MIPs.UofMD.landState.CMIP.UofMD-landState-2-1-h, version
870 20170126, *Earth Syst. Grid Fed.*, <http://doi.org/10.22033/ESGF/input4MIPs.1127>, 2017.

871 Jacobson, M.Z.: Investigating cloud absorption effects: global absorption properties of black
872 carbon, tar balls, and soil dust in clouds and aerosols. *J. Geophys. Res.* 117, D06205,
873 2012.

874 Jones, C.D., Arora, V., Friedlingstein, P., Bopp, L., Brovkin, V., Dunne, J., Graven, H.,
875 Hoffman, F., Ilyina, T., John, J. G., Jung, M., Kawamiya, M., Koven, C., Pongratz, J.,
876 Raddatz, T., Randerson, J. T., and Zaehle, S.: C4MIP – The Coupled Climate–Carbon
877 Cycle Model Intercomparison Project: experimental protocol for CMIP6, *Geosci. Model*
878 *Dev.*, 9, 2853–2880, doi:10.5194/gmd-9-2853-2016, 2016.

879 Lamarque, J.-F., Shindell, D. T., Josse, B., Young, P. J., Cionni, I., Eyring, V., Bergmann, D.,
880 Cameron-Smith, P., Collins, W. J., Doherty, R., Dalsoren, S., Faluvegi, G., Folberth, G.,
881 Ghan, S. J., Horowitz, L. W., Lee, Y. H., MacKenzie, I. A., Nagashima, T., Naik, V.,
882 Plummer, D., Righi, M., Rumbold, S. T., Schulz, M., Skeie, R. B., Stevenson, D. S.,
883 Strode, S., Sudo, K., Szopa, S., Voulgarakis, A., and Zeng, G.: The Atmospheric
884 Chemistry and Climate Model Intercomparison Project (ACCMIP): overview and
885 description of models, simulations and climate diagnostics, *Geosci. Model Dev.*, 6, 179–
886 206, doi:10.5194/gmd-6-179-2013, 2013.

887 Lamarque, J.-F., Emmons, L. K., Hess, P. G., Kinnison, D. E., Tilmes, S., Vitt, F., Heald, C.
888 L., Holland, E. A., Lauritzen, P. H., Neu, J., Orlando, J. J., Rasch, P. J., and Tyndall, G.
889 K.: CAM-chem: description and evaluation of interactive atmospheric chemistry in the
890 Community Earth System Model, *Geosci. Model Dev.*, 5, 369–411, 2012

891 Lamarque, J.-F., Bond, T. C., Eyring, V., Granier, C., Heil, A., Klimont, Z., Lee, D., Liousse,

892 C., Mieville, A., Owen, B., Schultz, M. G., Shindell, D., Smith, S. J., Stehfest, E., Van
893 Aardenne, J., Cooper, O. R., Kainuma, M., Mahowald, N., McConnell, J. R., Naik, V.,
894 Riahi, K., and van Vuuren, D. P.: Historical (1850–2000) gridded anthropogenic and
895 biomass burning emissions of reactive gases and aerosols: methodology and application,
896 *Atmos. Chem. Phys.*, 10, 7017-7039, <https://doi.org/10.5194/acp-10-7017-2010>, 2010.

897 [Lawrence, D. M., Hurtt, G. C., Arneeth, A., Brovkin, V., Calvin, K. V., Jones, A. D., Jones, C.](#)
898 [D., Lawrence, P. J., de Noblet-Ducoudré N., Pongratz, J., Seneviratne, S. I., and](#)
899 [Shevliakova, E.: The Land Use Model Intercomparison Project \(LUMIP\) contribution to](#)
900 [CMIP6: rationale and experimental design, *Geosci. Model Dev.*, 9, 2973–2998,](#)
901 <https://doi.org/10.5194/gmd-9-2973-2016>, 2016.

902 Lohmann, U., Feichter, J., Penner, J. E., and Leaitch, W. R.: Indirect effect of sulfate and
903 carbonaceous aerosols: A mechanistic treatment. *J. Geophys. Res.*, 105, 12193–12206,
904 2000

905 Li, W., Zhang, Y., Shi, X., Zhou, W., Huang, A., Mu, M., Qiu, B., Ji, J.: Development of the
906 Land Surface Model BCC_AVIM2.0 and Its Preliminary Performance in
907 LS3MIP/CMIP6, *J. Meteor. Res.*, 33(5), [851-869](#), doi: 10.1007/s13351-019-9016-y,
908 2019.

909 Liu, X. H., Penner, J. E., and Herzog, M.: Global modeling of aerosol dynamics: Model
910 description, evaluation, and interactions between sulfate and nonsulfate aerosols, *J.*
911 *Geophys. Res.-Atmos.*, 110, D18206, doi:10.1029/2004jd005674, 2005.

912 Liu, X., Easter, R.C. Ghan, S.J., Zaveri, R., Rasch, P., Shi, X., Lamarque, J.-F., Gettelman, A.,
913 Morrison, H., Vitt, F., Conley, A., Park, S., Neale, R., Hannay, C., Ekman, A.M., Hess,
914 P., Mahowald, N., Collins, W., Iacono, M.J., Bretherton, C.S., Flanner, M.G., and
915 Mitchell, D.: Toward a Minimal Representation of Aerosols in Climate Models:
916 Description and Evaluation in the Community Atmosphere Model CAM5.
917 *Geos.Model.Dev.* 5(3):709-739. 2012.

918 Liu, X., Ma, P. -L., Wang, H., Tilmes, S., Singh, B., Easter, R. C., Ghan, S. J., and Rasch, P.
919 J.: Description and evaluation of a new four-mode version of the Modal Aerosol Module
920 (MAM4) within version 5.3 of the Community Atmosphere Model, *Geosci. Model Dev.*,
921 9, 505–522, <https://doi.org/10.5194/gmd-9-505-2016>, 2016.

922 Liu, J., Mauzerall, D.L., Horowitz, L.W., Ginoux, P., Fiore, A.M.: Evaluation intercontinental
923 transport of fine aerosols: (1) methodology, global aerosol distribution and optical depth.

924 Atmos Environ 43:4327–4338, 2009.

925 Lu, X., Zhang, L., Wu, T., Long, M., Wang, J., Jacob, D., Zhang F., Zhang, J., Eastham, S.,
 926 Hu, L., Zhu, L., Liu, X., and Wei, M.: Development of the global atmospheric general
 927 circulation-chemistry model BCC-GEOS-Chem v1.0: model description and evaluation,
 928 submitted to Geos.Model.Dev.

929 Mahowald, N., Lamarque, J.-F., Tie, X., and Wolff, E.: Sea salt aerosol response to climate
 930 change: last glacial maximum, preindustrial and doubled carbon dioxide climates, J.
 931 Geophys. Res., 111, D05303, doi:10.1029/2005JD006459, 2006.

932 Martin, R. V., et al.: Interpretation of TOMS observations of tropical tropospheric ozone with
 933 a global model and in situ observations, J. Geophys. Res., 107(D18), 4351,
 934 doi:10.1029/2001JD001480, 2002.

935 Matsui, H., and Mahowald, N.: Development of a global aerosol model using a
 936 two-dimensional sectional method: 2. Evaluation and sensitivity simulations, J. Adv.
 937 Model. Earth Syst., 9, 1887 – 1920, doi:10.1002/2017MS000937, 2017.

938 Matthes, K., Funke, B., Andersson, M. E., Barnard, L., Beer, J., Charbonneau, P., Clilverd, M.
 939 A., Dudok de Wit, T., Haberreiter, M., Hendry, A., Jackman, C. H., Kretzschmar, M.,
 940 Kruschke, T., Kunze, M., Langematz, U., Marsh, D. R., Maycock, A. C., Misios, S.,
 941 Rodger, C. J., Scaife, A. A., Seppälä, A., Shangguan, M., Sinnhuber, M., Tourpali, K.,
 942 Usoskin, I., van de Kamp, M., Verronen, P. T., and Versick, S.: Solar forcing for CMIP6
 943 (v3.2), Geosci. Model Dev., 10, 2247–2302, <https://doi.org/10.5194/gmd-10-2247-2017>,
 944 2017.

945 Meinshausen, M., Vogel, E., Nauels, A., Lorbacher, K., Meinshausen, N., Etheridge, D. M.,
 946 Fraser, P. J., Montzka, S. A., Rayner, P. J., Trudinger, C. M., Krummel, P. B., Beyerle,
 947 U., Canadell, J. G., Daniel, J. S., Enting, I. G., Law, R. M., Lunder, C. R., O'Doherty, S.,
 948 Prinn, R. G., Reimann, S., Rubino, M., Velders, G. J. M., Vollmer, M. K., Wang, R. H. J.,
 949 and Weiss, R.: Historical greenhouse gas concentrations for climate modelling (CMIP6),
 950 Geosci. Model Dev., 10, 2057–2116, <https://doi.org/10.5194/gmd-10-2057-2017>, 2017.

951 Mora, C., Wei, C.-L., Rollo, A., Amaro, T., Baco, A.R., Billett, D., Bopp, L., Chen, Q.,
 952 Collier, M., Danovaro, R., Gooday, A.J., Grube, B.M., Halloran, P.R., Ingels, J., Jones,
 953 D.O.B., Levin, L.A., Nakano, H., Norling, K., Ramirez-Llodra, E., Rex, M., Ruh, H.A.,
 954 Smith, C.R., Sweetman, A.K., Thurber, A.R., Tjiputra, J. F., Usseglio, P., Watling, L.,
 955 Wu, T., Yasuhara, M.: Biotic and human vulnerability to projected ocean

956 biogeochemistry change over the 21st century, *PLoS Biol* 11(10): e1001682.
957 doi:10.1371/journal.pbio.1001682, 2013.

958 NCAR Command Language (Version 6.6.2) [Software], Boulder, Colorado:
959 UCAR/NCAR/CISL/TDD. <http://dx.doi.org/10.5065/D6WD3XH5>, 2019.

960 Neale, R. B., et al.: Description of the NCAR Community Atmosphere Model (CAM 4.0),
961 NCAR Tech. Note, TN-485, pp. 212, Natl. Cent. for Atmos. Res., Boulder, Colo., 2010

962 Neu, J. L. and Prather, M. J.: Toward a more physical representation of precipitation
963 scavenging in global chemistry models: cloud overlap and ice physics and their impact
964 on tropospheric ozone, *Atmos. Chem. Phys. Discuss.*, 11, 24413–24466,
965 doi:10.5194/acpd-11-24413-2011, 2011.

966 Olivier, J.G.J., Bouwman, A.F., Van der Maas, C.W.M., Berdowski, J.J.M., Veldt, C., Bloos,
967 J.P.J., Visschedijk, A.J.H., Zandveld, P.Y.J., Haverslag, J.L., Description of EDGAR
968 Version 2.0: A set of global emission inventories of greenhouse gases and ozone
969 depleting substances for all anthropogenic and most natural sources on a per country
970 basis and on 1° x 1° grid. RIVM Techn. Report nr. 771060002, TNO-MEP report nr.
971 R96/119. Nat. Inst. Of Public Health and the Environment/ Netherlands Organisation for
972 Applied Scientific Research, Bilthoven, 1996.

973 Peng, Y., and Lohmann, U.: Sensitivity study of the spectral dispersion of the cloud droplet
974 size distribution on the indirect aerosol effect, *Geophys. Res. Lett.*, 30(10), 1507,
975 doi:10.1029/2003GL017192, 2003.

976 Price, C., and Rind, D.: A simple lightning parameterization for calculating global lightning
977 distributions, *J. Geophys. Res.*, 97, 9919-9933, 1992.

978 Quaas, J., Boucher, O., and Lohmann, U.: Constraining the total aerosol indirect effect in
979 the LMDZ and ECHAM4 GCMs using MODIS satellite data. *Atmos Chem Phys* 6,947–
980 955, 2006.

981 Sander, S., Friedl, R. R., Ravishankara, A. R., et al.: Chemical Kinetics and Photochemical
982 Data for Use in Atmospheric Studies, Evaluation Number 14, JPL Publication 02-25,
983 NASA, Jet Propulsion Laboratory, California Institute of Technology, Pasadena, CA,
984 2003.

985 Schlesinger, M. E., Mintz, Y.: Numerical simulation of ozone production, transport and
986 distribution with a global atmospheric general circulation model, *J.Atmos.Sci.*, 36:

987 1325-1361, 1979.

988 Shindell, D.T., Horowitz, L.W., Schwarzkopf, M.D.: Composition Models in Climate
989 Projections Based on Emissions Scenarios for Long-Lived and Short-Lived Radiatively
990 Active Gases and Aerosols. H.Levy II, D.T. Shindell, A.Gilliland, M.D.Schwarzkopf,
991 L.W.Horowitz, (eds.) .A Report by the U.S.Climate Change Science Program and the
992 Subcommittee on Global Change Research, Washington, D.C., 2008

993 Solomon, S.: Stratospheric ozone depletion: A review of concepts and history, *Reviews of*
994 *Geophysics*, 37, 275–316, 1999.

995 Taylor, K.E., Stouffer, R. J., Meehl, G. A.: An overview of CMIP5 and the experiment design,
996 *Bull. Am. Meteorol. Soc.* 93, 485-498, 2012.

997 Tegen, I., Neubauer, D., Ferrachat, S., Siegenthaler-Le Drian, C., Bey, I., Schutgens, N., Stier,
998 P., Watson-Parris, D., Stanelle, T., Schmidt, H., Rast, S., Kokkola, H., Schultz, M.,
999 Schroeder, S., Daskalakis, N., Barthel, S., Heinold, B., and Lohmann, U.: The global
1000 aerosol–climate model ECHAM6.3–HAM2.3 – Part 1: Aerosol evaluation, *Geosci.*
1001 *Model Dev.*, 12, 1643–1677, <https://doi.org/10.5194/gmd-12-1643-2019>, 2019.

1002 Textor, C., Schulz, M., Guibert, S., Kinne, S., Balkanski, Y., Bauer, S., Berntsen, T., Berglen,
1003 T., Boucher, O., Chin, M., Dentener, F., Diehl, T., Easter, R., Feichter, H., Fillmore, D.,
1004 Ghan, S., Ginoux, P., Gong, S., Grini, A., Hendricks, J., Horowitz, L., Huang, P., Isaksen,
1005 I., Iversen, I., Kloster, S., Koch, D., Kirkevåg, A., Kristjansson, J. E., Krol, M., Lauer, A.,
1006 Lamarque, J. F., Liu, X., Montanaro, V., Myhre, G., Penner, J., Pitari, G., Reddy, S.,
1007 Seland, Ø., Stier, P., Takemura, T., and Tie, X.: Analysis and quantification of the
1008 diversities of aerosol life cycles within AeroCom, *Atmos. Chem. Phys.*, 6, 1777–1813,
1009 <https://doi.org/10.5194/acp-6-1777-2006>, 2006.

1010 Thomason, L. W., Ernest, N., Millán, L., Rieger, L., Bourassa, A., Vernier, J. P., Manney, G.,
1011 Luo, B.P., Arfeuille, F., Peter, T.: A global space - based stratospheric aerosol
1012 climatology: 1979-2016. *Earth System Science Data*, 10(1), 469–492, doi:
1013 10.5194/essd-10-469-2018, 2018.

1014 Tie, X., Brasseur, G., Emmons, L., Horowitz, L., and Kinnison, D.: Effects of aerosols on
1015 tropospheric oxidants: A global model study, *J. Geophys. Res.*, 106, 2931– 2964, 2001.

1016 Tie, X., Madronich, S., Walters, S., Edwards, D., Ginoux, P., Mahowald, N., Zhang, R., Luo,
1017 C., and Brasseur, G.: Assessment of the global impact of aerosols on tropospheric
1018 oxidants, *J. Geophys. Res.*, 110, D03204, doi:10.1029/2004JD005359, 2005.

1019 Tilmes, S., Lamarque, J.-F., Emmons, L. K., Kinnison, D. E., Marsh, D., Garcia, R. R., Smith,
1020 A. K., Neely, R. R., Conley, A., Vitt, F., Val Martin, M., Tanimoto, H., Simpson, I.,
1021 Blake, D. R., and Blake, N.: Representation of the Community Earth System Model
1022 (CESM1) CAM4-chem within the Chemistry-Climate Model Initiative (CCMI),
1023 Geoscientific Model Development, 9, 1853-1890, 2016.

1024 Todd-Brown, K.E.O., Randerson, J.T., Hopkins, F., Arora, V., Hajima, T., Jones, C.,
1025 Shevliakova, E., Tjiputra, J., Volodin, E., Wu, T., Zhang, Q., Allison, S.D.: Changes in
1026 soil organic carbon storage predicted by Earth system models during the 21st century,
1027 Biogeosciences, 11, 2341-2356, 2014.

1028 [Van Marle, M.J.E., S. Kloster, B.I. Magi, J.R. Marlon, A.-L. Daniau, R.D. Field, A. Arneeth,](#)
1029 [M. Forrest, S. Hantson, N.M. Kehrwald, W. Knorr, G. Lasslop, F. Li, S. Mangeon, C.](#)
1030 [Yue, J.W. Kaiser, and G.R. van der Werf, 2017: Historic global biomass burning](#)
1031 [emissions for CMIP6 \(BB4CMIP\) based on merging satellite observations with proxies](#)
1032 [and fire models \(1750-2015\). Geosci. Model Dev., 10, 3329-3357,](#)
1033 [doi:10.5194/gmd-10-3329-2017.](#)

1034 Wang, J., Hoffmann, A. A., Park, R., Jacob, D. J., and Martin, S. T.: Global distribution of
1035 solid and aqueous sulfate aerosols: effect of the hysteresis of particle phase transitions, J.
1036 Geophys. Res., 113, D11206, Doi:11210.11029/12007JD009367, 2008a.

1037 Wang, J., Jacob, D. J., and Martin, S. T.: Sensitivity of sulfate direct climate forcing to the
1038 hysteresis of particle phase transitions, J. Geophys. Res., 113, D11207,
1039 doi:11210.11029/12007JD009368, 2008b.

1040 Wesely, M. L.: Parameterization of surface resistance to gaseous dry deposition in
1041 regional-scale numerical models, Atmos. Environ., 23, 1293–1304, 1989.

1042 Wild, M., Folini, D., Schar, C., Loeb, N., Dutton, E.G., Konig-Langlo, G.: The global energy
1043 balance from a surface perspective, Climate Dynamics, 40: 3107-3134, 2013.

1044 Williamson, D. L., and Rasch, P. J.: Two-dimensional semi-Lagrangian transport with
1045 shapepreserving interpolation, Mon. Wea. Rev., 117, 102–129, 1989.

1046 Wofsy, S. C. and the HIPPO team: HIAPER Pole-to-Pole Observations (HIPPO): fine-grained,
1047 global-scale measurements of climatically important atmospheric gases and aerosols,
1048 Philo T. R. Soc. A, 369, 2073–86, doi:10.1098/rsta.2010.0313, 2011.

1049 Wu, T., Song, L., Li, W., Wang, Z., Zhang, H., Xin, X., Zhang, Y., Zhang, L., Li, J., Wu, F.,
1050 Liu, Y., Zhang, F., Shi, X., Chu, M., Zhang, J., Fang, Y., Wang, F., Lu, Y., Liu, X., Wei,

1051 M., Liu, Q., Zhou, W., Dong, M., Zhao, Q., Ji, J., Li, L., Zhou, M.: An overview of BCC
1052 climate system model development and application for climate change studies. *J. Meteor.*
1053 *Res.*, 28(1), 34-56, 2014.

1054 Wu, T., Li, W., Ji, J., Xin, X., Li, L., Wang, Z, Zhang, Y., Li, J., Zhang, F., Wei, M., Shi, X.,
1055 Wu, F., Zhang, L., Chu, M., Jie, W., Liu, Y., Wang, F., Liu, X., Li, Q., Dong, M., Liang,
1056 X., Gao, Y., Zhang, J.: Global carbon budgets simulated by the Beijing climate center
1057 climate system model for the last century. *J Geophys Res Atmos*, 118, 4326-4347. doi:
1058 10.1002/jgrd.50320, 2013.

1059 Wu, T., Lu, Y., Fang, Y., Xin, X., Li, L., Li, W., Jie, W., Zhang, J., Liu, Y., Zhang, L., Zhang,
1060 F., Zhang, Y., Wu, F., Li, J., Chu, M., Wang, Z., Shi, X., Liu, X., Wei, M., Huang, A.,
1061 Zhang, Y., and Liu, X.: The Beijing Climate Center Climate System Model (BCC-CSM):
1062 the main progress from CMIP5 to CMIP6, *Geos.Model Dev.*, 12, 1573-1600,
1063 <http://doi.org/10.5194/gmd-12-1573-2019>, 2019.

1064 Young, P. J., Archibald, A. T., Bowman, K. W., Lamarque, J. F., Naik, V., Stevenson, D. S.,
1065 Tilmes, S., Voulgarakis, A., Wild, O., Bergmann, D., Cameron-Smith, P., Cionni, I.,
1066 Collins, W. J., Dalsøren, S. B., Doherty, R. M., Eyring, V., Faluvegi, G., Horowitz, L.
1067 W., Josse, B., Lee, Y. H., MacKenzie, I. A., Nagashima, T., Plummer, D. A., Righi, M.,
1068 Rumbold, S. T., Skeie, R. B., Shindell, D. T., Strode, S. A., Sudo, K., Szopa, S., and
1069 Zeng, G.: Pre-industrial to end 21st century projections of tropospheric ozone from the
1070 Atmospheric Chemistry and Climate Model Intercomparison Project (ACCMIP), *Atmos.*
1071 *Chem. Phys.*, 13, 2063-2090, <http://doi.org/10.5194/acp-13-2063-2013>, 2013.

1072 Young, P. J., Naik, V., Fiore, A. M., Gaudel, A., Guo, J., Lin, M. Y., Neu, J. L., Parrish, D. D.,
1073 Rieder, H. E., Schnell, J. L., Tilmes, S., Wild, O., Zhang, L., Ziemke, J. R., Brandt, J.,
1074 Delcloo, A., Doherty, R. M., Geels, C., Hegglin, M. I., Hu, L., Im, U., Kumar, R., Luhar,
1075 A., Murray, L., Plummer, D., Rodriguez, J., Saiz-Lopez, A., Schultz, M. G., Woodhouse,
1076 M. T., and Zeng, G.: Tropospheric Ozone Assessment Report: Assessment of
1077 global-scale model performance for global and regional ozone distributions, variability,
1078 and trends, *Elem Sci Anth*, 6, 10, <http://doi.org/10.1525/elementa.265>, 2018.

1079 Zender, C., Bian, H., and Newman, D.: Mineral Dust Entrainment and Deposition (DEAD)
1080 model: Description and 1990s dust climatology, *J. Geophys. Res.*, 108(D14), 4416, doi:
1081 10.1029/2002JD002775, 2003.

1082 [Zhang, J., Wu, T., Shi, X., Zhang F., Li, J., Chu, M., Liu, Q., Yan, J., Ma, Q., Wei, M.: BCC](#)

1083 | BCC-ESM1 model output prepared for CMIP6 AerChemMIP. Version
1084 | YYYYMMDD[1], Earth System Grid Federation,
1085 | <https://doi.org/10.22033/ESGF/CMIP6.1733>, 2019.
1086

1087 Table 1. Chemical species considered in BCC-AGCM3-Chem. Species marked with star (*)
 1088 denote those added in BCC-ESM1 apart from the 63 species used in MOZART2. In the
 1089 column of surface emission, interactive surface emissions are considered for sea salt and dust.
 1090

Species	Dry deposition	Wet deposition	Surface emission	Aircraft emission	Volcanic emission
O ₃	✓				
N ₂ O			✓		
N					
NO	✓		✓	✓	
NO ₂	✓				
NO ₃					
HNO ₃	✓	✓			
HO ₂ NO ₂	✓	✓			
N ₂ O ₅					
CH ₄	✓		✓	✓	
CH ₃ O ₂					
CH ₃ OOH	✓	✓			
CH ₂ O	✓	✓	✓		
CO	✓		✓	✓	
OH					
HO ₂					
H ₂ O ₂	✓	✓			
C ₃ H ₆			✓		
ISOP			✓		
Gas tracers					
PO ₂					
CH ₃ CHO	✓	✓	✓		
POOH	✓	✓			
CH ₃ CO ₃					
CH ₃ COOOH	✓	✓			
PAN	✓				
ONIT	✓	✓			
C ₂ H ₆			✓		
C ₂ H ₄			✓		
C ₄ H ₁₀			✓		
MPAN	✓				
ISOPO ₂					
MVK		✓			
MACR		✓			
MACRO ₂					
MACROOH	✓	✓			
MCO ₃					
C ₂ H ₅ O ₂					
C ₂ H ₅ OOH	✓	✓			
C ₁₀ H ₁₆			✓		

1091

1092

Table 1. Continued.

Species name	Dry deposition	Wet deposition	Surface emission	Aircraft emission	Volcanic emission
C ₃ H ₈			✓		
C ₃ H ₇ O ₂					
C ₃ H ₇ OOH	✓	✓			
CH ₃ COCH ₃	✓		✓		
ROOH		✓			
CH ₃ OH	✓	✓	✓		
C ₂ H ₅ OH	✓	✓	✓		
GLYALD	✓	✓			
HYAC	✓	✓			
EO ₂					
EO					
HYDRALD	✓	✓			
RO ₂					
CH ₃ COCHO	✓	✓	✓		
Rn-222					
Pb-210	✓	✓			
ISOPNO ₃		✓			
ONITR	✓	✓			
XO ₂					
XOOH	✓	✓			
ISOPOOH	✓	✓			
H ₂	✓		✓		
Stratospheric O ₃	✓				
Inert O ₃	✓				
SO ₂ *	✓	✓	✓	✓	✓
DMS*			✓		
NH ₃ *			✓	✓	
SO ₄ ²⁻ *	✓	✓			
OC1*	✓	✓	✓	✓	
OC2*	✓	✓	✓	✓	
BC1*	✓	✓	✓	✓	
BC2*	✓	✓	✓	✓	
SSLT01*	✓	✓			
SSLT02*	✓	✓			
SSLT03*	✓	✓			
SSLT04*	✓	✓			
DST01*	✓	✓			
DST02*	✓	✓			
DST03*	✓	✓			
DST04*	✓	✓			

1096 Table 2. Gas-phase chemical reactions for NH₃ and bulk aerosols precursors following
 1097 CAM-Chem (Lamarque et al., 2012). The reaction rates (s⁻¹) refer to Tie et al. (2001) and
 1098 Sander et al. (2003), and Cooke and Wilson (1996). Temperature (T) is expressed in K, air
 1099 density (M) in molecule cm⁻³, ki and ko in cm³ molecule⁻¹ s⁻¹.
 1100

Chemical reactions	Rate
NH ₃ + OH → H ₂ O	1.70E-12*exp(-710/T)
SO ₂ + OH → SO ₄ ²⁻	ko/(1.+ko*M/ki)*f**(1./(1.+log10(ko*M/ki))), in which ko=3.0E-31*(300/T)**3.3; ki=1.E-12; f=0.6
DMS + OH → SO ₂	9.60E-12*exp(-234./T)
DMS + OH → .5*SO ₂ + .5*HO ₂	1.7E-42*exp(7810/T)*M*0.21/(1+5.5E-31*exp(7460/T)* M* 0.21)
DMS + NO ₃ → SO ₂ + HNO ₃	1.90E-13*exp(520/T)
BC1 → BC2	7.10E-06
OC1 → OC2	7.10E-06

1101
 1102

1103

1104

1105

Table 3. Size and density parameters of bulk aerosols.

Aerosols	Species Name	Mean radius (μm) / bin size (μm)	Geometric standard deviation (μm)	Density (g cm^{-3})
SO_4^{2-}	Sulfate	0.05	2.03	1.77
BC1	hydrophobic black carbon	0.02	2.00	1.0
BC2	hydrophilic black carbon	0.02	2.00	1.0
OC1	hydrophobic organic carbon	0.03	2.24	1.8
OC2	hydrophilic organic carbon	0.03	2.24	1.8
DST01	Dust	0.55 / bin: 0.1-1.0	2.00	2.5
DST02	Dust	1.75 / bin: 1.0-2.5	2.00	2.5
DST03	Dust	3.75 / bin: 2.5-5.0	2.00	2.5
DST04	Dust	7.50 / bin: 5.0-10.	2.00	2.5
SSLT01	Sea salt	0.52 / bin: 0.2-1.0	2.00	2.2
SSLT02	Sea salt	2.38 / bin: 1.0-3.0	2.00	2.2
SSLT03	Sea salt	4.86 / bin: 3.0-10.	2.00	2.2
SSLT04	Sea salt	15.14 / bin: 10.-20.	2.00	2.2

1106

Table 4. Source of emission data. MOZART2 data denote the standard tropospheric chemistry package for MOZART contains surface emissions from the EDGAR 2.0 data base (Olivier et al., 1996). ACCMIP data are downloaded from the IPCC ACCMIP emission inventory (<http://accent.aero.jussieu.fr/ACCMIP.php>) and they vary from 1850 to 2000, in 10-year steps (Lamarque et al., 2010). CMIP6 data are from <https://esgf-node.llnl.gov/search/input4mips/>. Anthropogenic emission includes Industrial and fossil fuel use, agriculture, ships, and etc. Biomass burning includes vegetation fires incl. fuel wood and agricultural burning.

Species	Anthropogenic emission	Biomass burning	Biogenic emissions from vegetation	Biogenic emissions from soil	Oceanic emissions	Airplane emission	Volcanic emission
C ₂ H ₄	CMIP6	CMIP6	On-line computation		MOZART2		
C ₂ H ₅ OH	CMIP6	CMIP6					
C ₂ H ₆	CMIP6	CMIP6	ACCMIP		MOZART2		
C ₃ H ₆	CMIP6	CMIP6	On-line computation		MOZART2		
C ₃ H ₈	CMIP6	CMIP6	ACCMIP		MOZART2		
C ₄ H ₁₀	CMIP6	CMIP5	MOZART2		MOZART2		
CH ₂ O	CMIP6	CMIP6					
CH ₃ CHO	ACCMIP	CMIP6					
CH ₃ COCHO		CMIP6					
CH ₃ OH	ACCMIP	CMIP6	ACCMIP				
CH ₃ COCH ₃	ACCMIP	ACCMIP	On-line computation		MOZART2		
ISOP		CMIP5	On-line computation				
C ₁₀ H ₁₆		CMIP6	On-line computation				
CH ₄	CMIP6	CMIP6	MOZART2		MOZART2	CMIP6	
CO	CMIP6	CMIP6	ACCMIP	MOZART2	ACCMIP	CMIP6	
H ₂	MOZART2	CMIP6		MOZART2	MOZART2		
N ₂ O	MOZART2	CMIP6		MOZART2	MOZART2		
NH ₃	CMIP6	CMIP6		ACCMIP	ACCMIP	CMIP6	
NO	CMIP6	CMIP6		ACCMIP		CMIP6	
SO ₂	CMIP6	CMIP6				CMIP6	ACCMIP
DMS					ACCMIP		
OC1	CMIP6	CMIP6				CMIP6	
OC2	CMIP6	CMIP6	On-line computation			CMIP6	
BC1	CMIP6	CMIP6				CMIP6	
BC2	CMIP6	CMIP6				CMIP6	

Table 5. Global budgets for DMS, SO₂, and sulfate in the period of 1991 to 2000. Units are sources and sinks, Tg(S) yr⁻¹; burden, Tg; lifetime, days.

		BCC-ESM (1991-2000 mean)	Other studies and CMIP5 data
DMS	Sources	27.4	
	Emission	27.4	10.7-23.7 ^a
	Sinks	28.0	
	Gas-phase oxidation	28.0	
	Burden	0.12	0.04-0.29 ^a
	Lifetime	0.78	0.5-3.0 ^a
SO ₂	Sources	76.93	
	Emission at surface	63.63	
	Emission from airplane	0.10	
	DMS oxidation	13.20	10.0-24.7 ^a
	Sinks	76.96	
	Dry deposition	18.53	16.0-55.0 ^a
	Wet deposition	9.36	0.0-19.9 ^a
	Gas-phase oxidation	10.33	6.1-16.8 ^a
	Aqueous-phase oxidation	38.74	24.5-57.8 ^a
Burden	0.48	0.40-1.22 ^a	
Lifetime	1.12	0.6-2.6 ^a	
SO ₄ ²⁻	Sources	49.05	59.67 ± 13.13 ^b
	Emission	0.00	
	SO ₂ aqueous-phase oxidation	38.73	
	SO ₂ gas-phase oxidation	10.32	
	Sinks	49.06	
	Dry deposition	2.20	4.96-5.51 ^d
	Wet deposition	46.86	39.34-40.20 ^d
	Burden	1.89	1.98 ± 0.48 ^b , 1.71 ^c , 1.2 ^g , 2.22-2.43 ^h
	Lifetime	4.69	4.12 ± 0.74 ^b , 3.72-3.77 ^d 3.3 ^g , 3.7-4.0 ^h

Notes: References denote a for Liu et al. (2005), b for Textor et al. (2006), c for the values derived from CMIP5 prescribed aerosol masses averaged from 1991 to 2000, d for Liu et al. (2012), g for Matsui and Mahowald (2017), and h for Tegen et al. (2019). Values of DMS, SO₂, and sulfate burdens in the literature d are transferred from TgS to Tg (species) for units consistence.

Table 6. Same as Table 5, but for global budgets for black carbon, organic carbon, dust, and sea salts. Units are sources and sinks, Tg yr⁻¹; burden, Tg; lifetime, days.

		BCC-ESM (1991-2000 mean)	Other studies and CMIP5 data
BC	Sources	7.22	
	Emission	7.22	11.9 ± 2.7 ^b , 7.8 ^g
	Sinks	7.24	7.75 ^d , 7.8 ^g
	Dry deposition	0.90	0.27 ^g , 1.30-1.64 ^e
	Wet deposition	6.34	7.5 ^g , 6.10-6.45 ^e
	Burden	0.13	0.114 ^c , 0.24 ± 0.1 ^b , 0.11 ^g , 0.14-0.26 ^h , 0.084-0.123 ^e
	Lifetime	6.60	7.12 ± 2.35 ^b , 3.95-4.80 ^e , 5.0 ^g , 6.3-7.5 ^h
OC	Sources	32.29	
	Fossil and biofuel emission	13.91	
	Natural emission	18.38	
	Sinks	32.30	
	Dry deposition	2.44	
	Wet deposition	29.86	
	Burden	0.62	0.69 ^c , 1.7 ± 0.45 ^b , 1.0-2.2 ^h
Lifetime	5.00	6.54 ± 1.76 ^b , 4.56-4.90 ^d , 6.4 ^g , 5.4-6.6 ^h	
Dust	Sources	2592.0	1840 ^b , 2943.5-3121.9 ^d , 2677 ^g
	Sinks	2592.0	
	Dry deposition	1630.8	1444 ^g
	Wet deposition	961.2	1245 ^g
	Burden	22.93	20.41 ^c , 22.424.7 ^d , 35.9 ^f , 19.2 ± 7.68 ^b , 28.5 ^g , 16.5-17.9 ^h
	Lifetime	3.23	4.14 ± 1.78 ^b , 2.61-3.07 ^d , 3.9 ^g , 5.3-5.7 ^h
Sea Salt	Sources	4667.2	4965.5-5004.1 ^d , 5039 ^g
	Sinks	4667.4	
	Dry deposition	2978.5	2158 ^g
	Wet deposition	1688.9	2918 ^g
	Burden	11.89	7.58-10.37 ^a , 6.4 ± 3.4 ^b , 11.84 ^c , 13.6 ^g , 3.9 ^h
	Lifetime	0.93	0.41 ± 0.24 ^b , 0.55-0.76 ^d , 0.98 ^g , 1.2-1.3 ^h

Notes: References denote a for Liu et al. (2005), b for Textor et al. (2006), c derived from CMIP5 prescribed aerosol masses averaged from 1991 to 2000, d for Liu et al. (2012), e for Liu et al. (2016), f for Ginoux (2001), g for Matsui and Mahowald (2017), and h for Tegen et al. (2019).

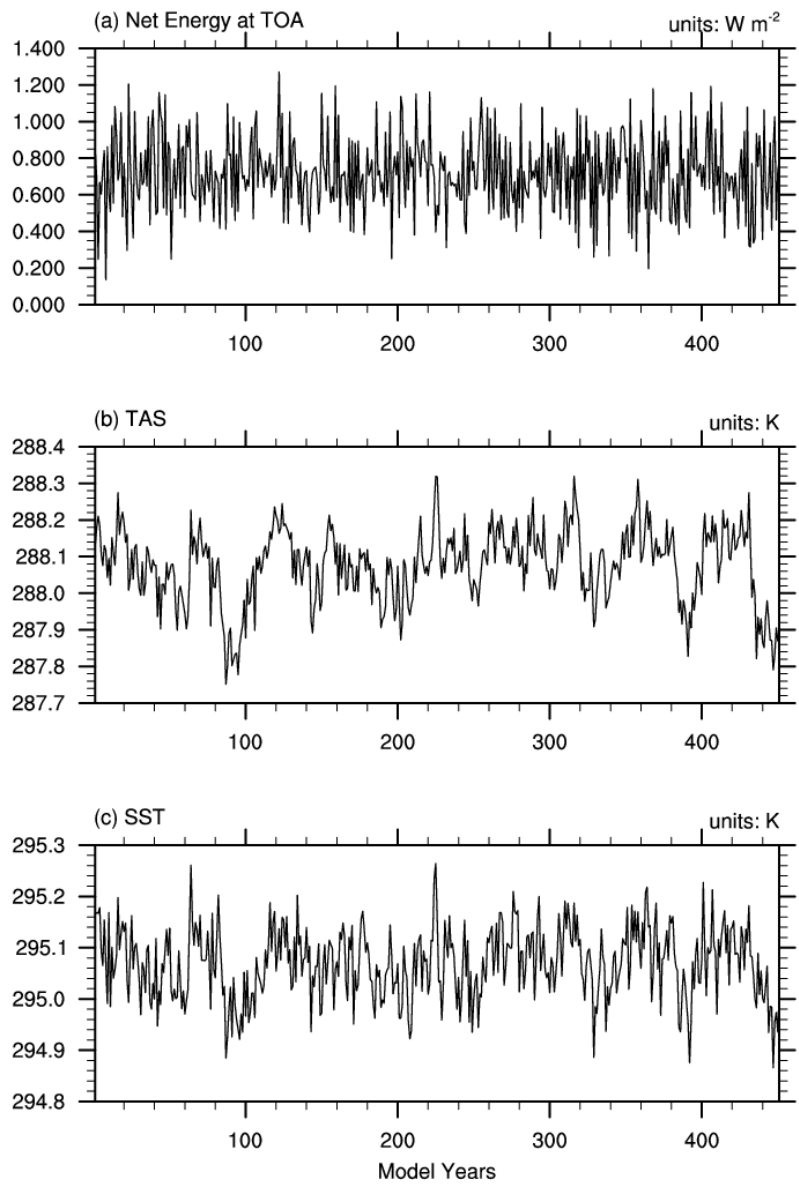


Figure 1. The time series of global and annual mean of (a) net energy budget at top of atmosphere ($W m^{-2}$), (b) near-surface air temperature (K), and (c) sea surface temperature (K) in the last 450 years of the piControl simulation.

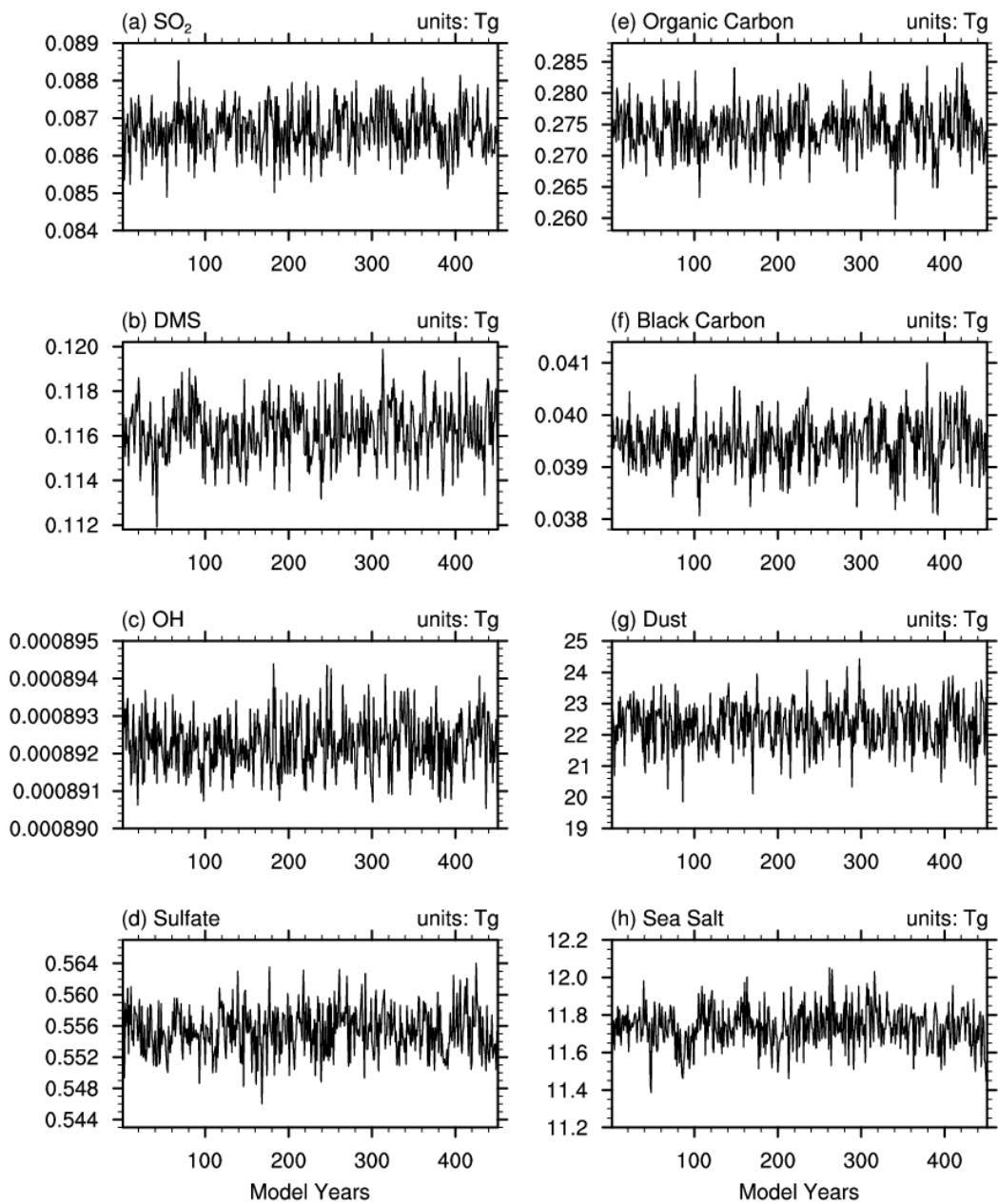


Figure 2. Same as in Figure 1, but for the global burdens of (a) SO_2 , (b) DMS, (c) OH, and (d-h) different aerosols in the troposphere (below 100 hPa). Units are Tg.

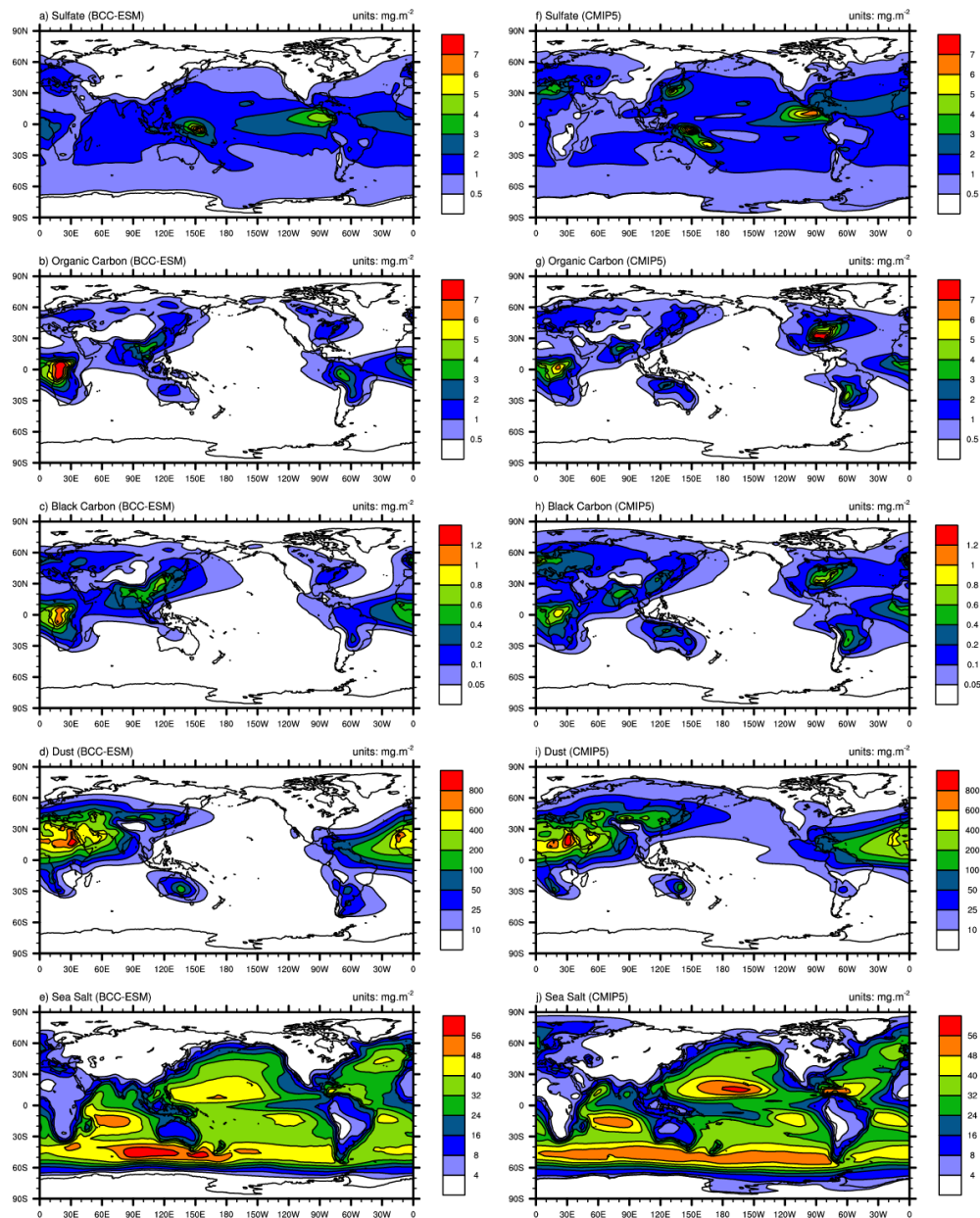


Figure 3. Global distributions of annual mean mass burdens of sulfate (SO_4^{2-} ; first row), organic carbon (OC; second row), black carbon (BC; third row), dust (fourth row), and sea salt (fifth row) aerosols in the whole atmospheric column. The left panels show the mean averaged for the last 100 years of BCC-ESM pre-industrial piControl simulations, and the right panels show the CMIP5 recommended aerosol concentrations in year 1850 (the website at IASA <http://tntcat.iiasa.ac.at/RcpDb/>). Units: mg m^{-2} .

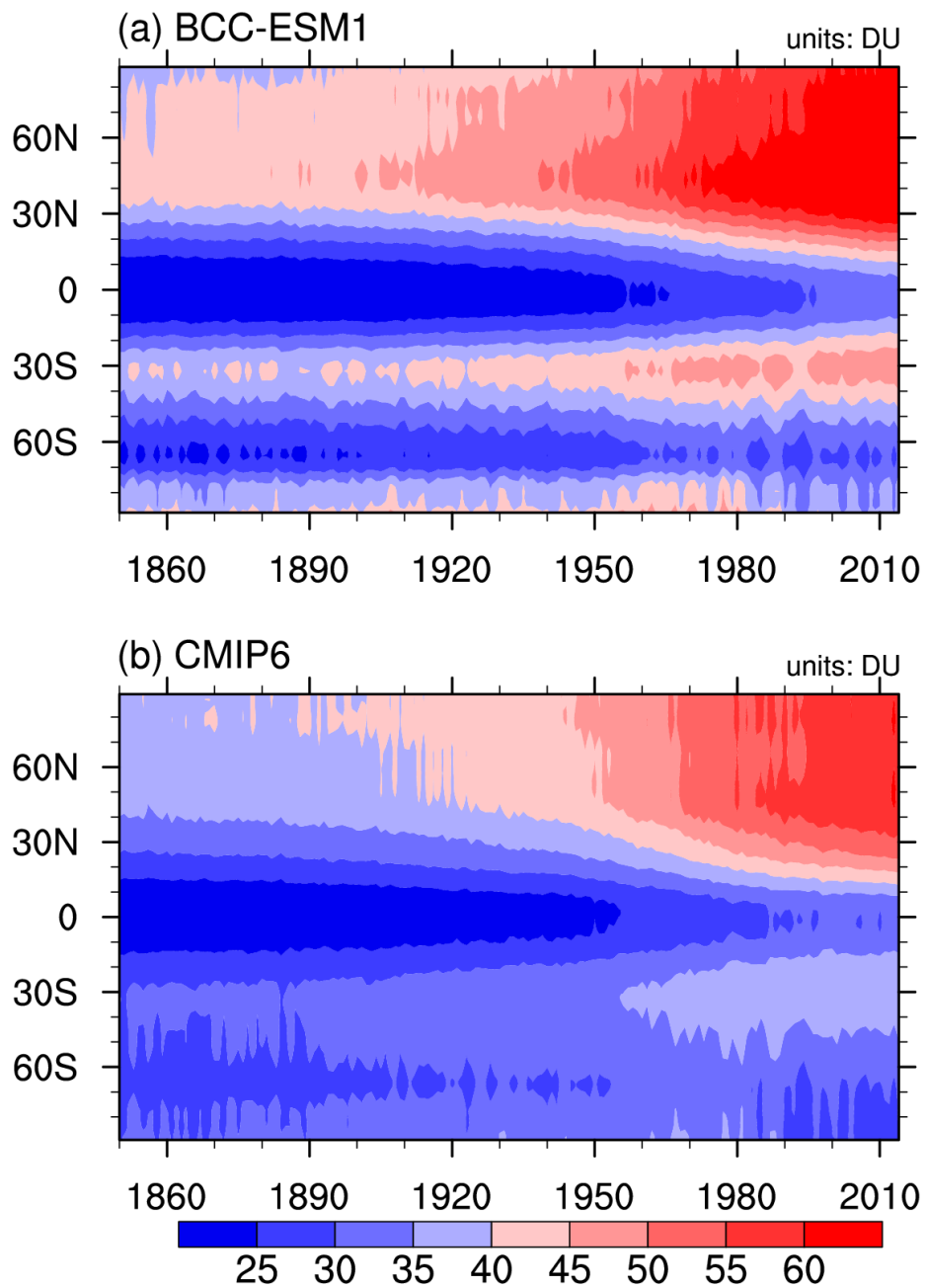


Figure 4. Zonal mean of yearly mean concentration of ozone column in the troposphere below 300 hPa to the ground from 1871 to 1999 for (a) BCC-ESM1 and (b) CMIP6 data. Unit: DU.

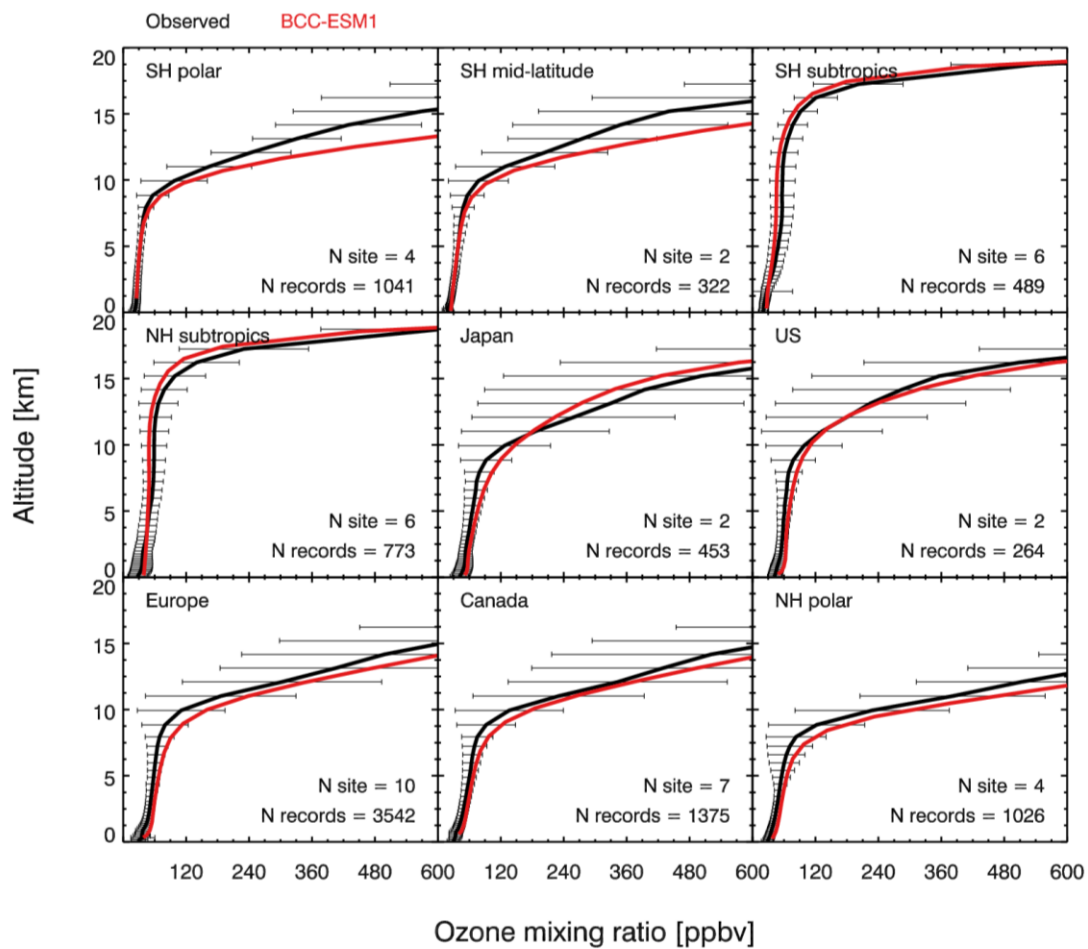


Figure 5. Vertical profiles of annual mean ozone concentrations from observations averaged for 2010-2014 in nine regions (black) and from the BCC-ESM1 simulations (red). The observations are derived from 41 global WOUDC sites.

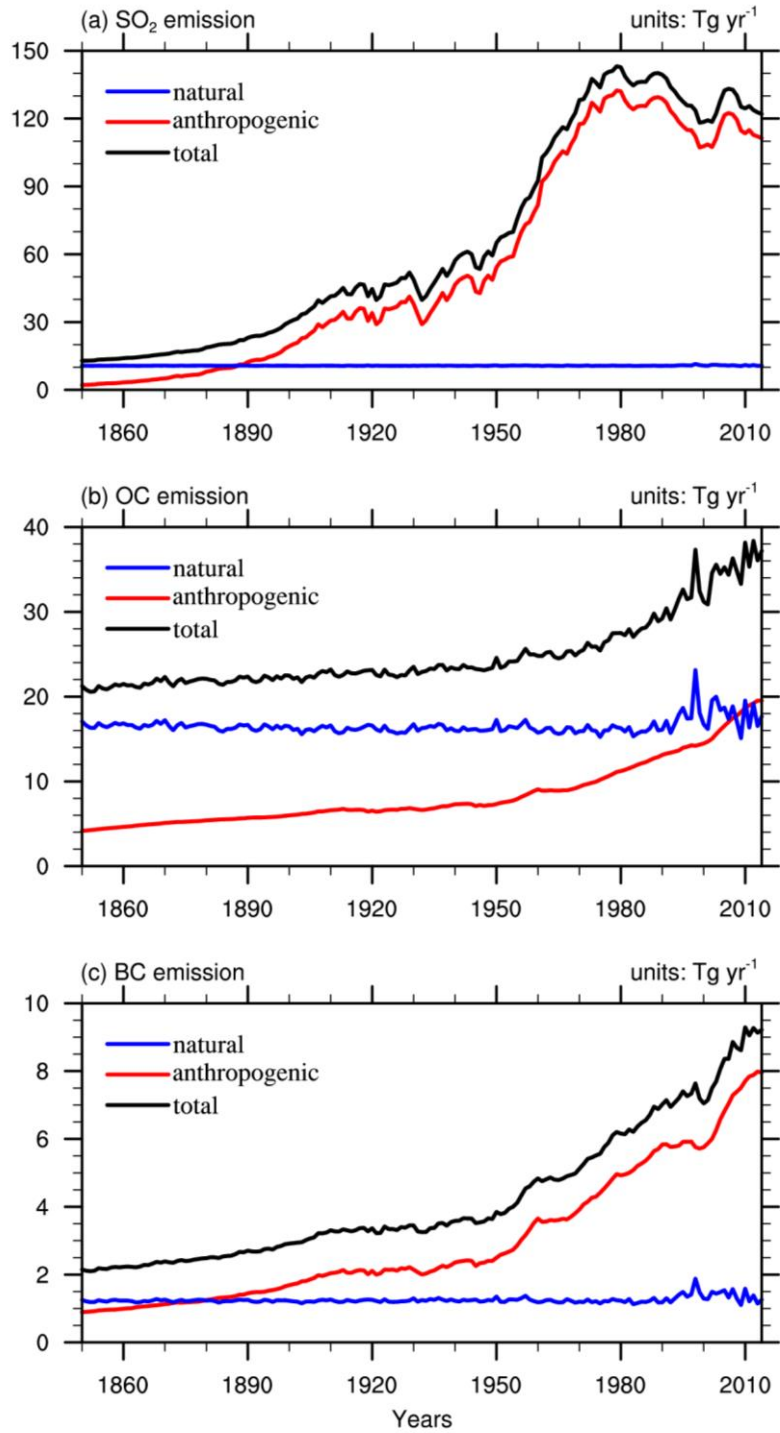


Figure 6. Global annual anthropogenic, natural, and total emissions of SO₂, organic carbon (OC), and black carbon (BC) in the BCC-ESM1 historical simulation. All the biomass burning emissions are included in natural emissions in (a)-(c). Units: Tg yr^{-1} .

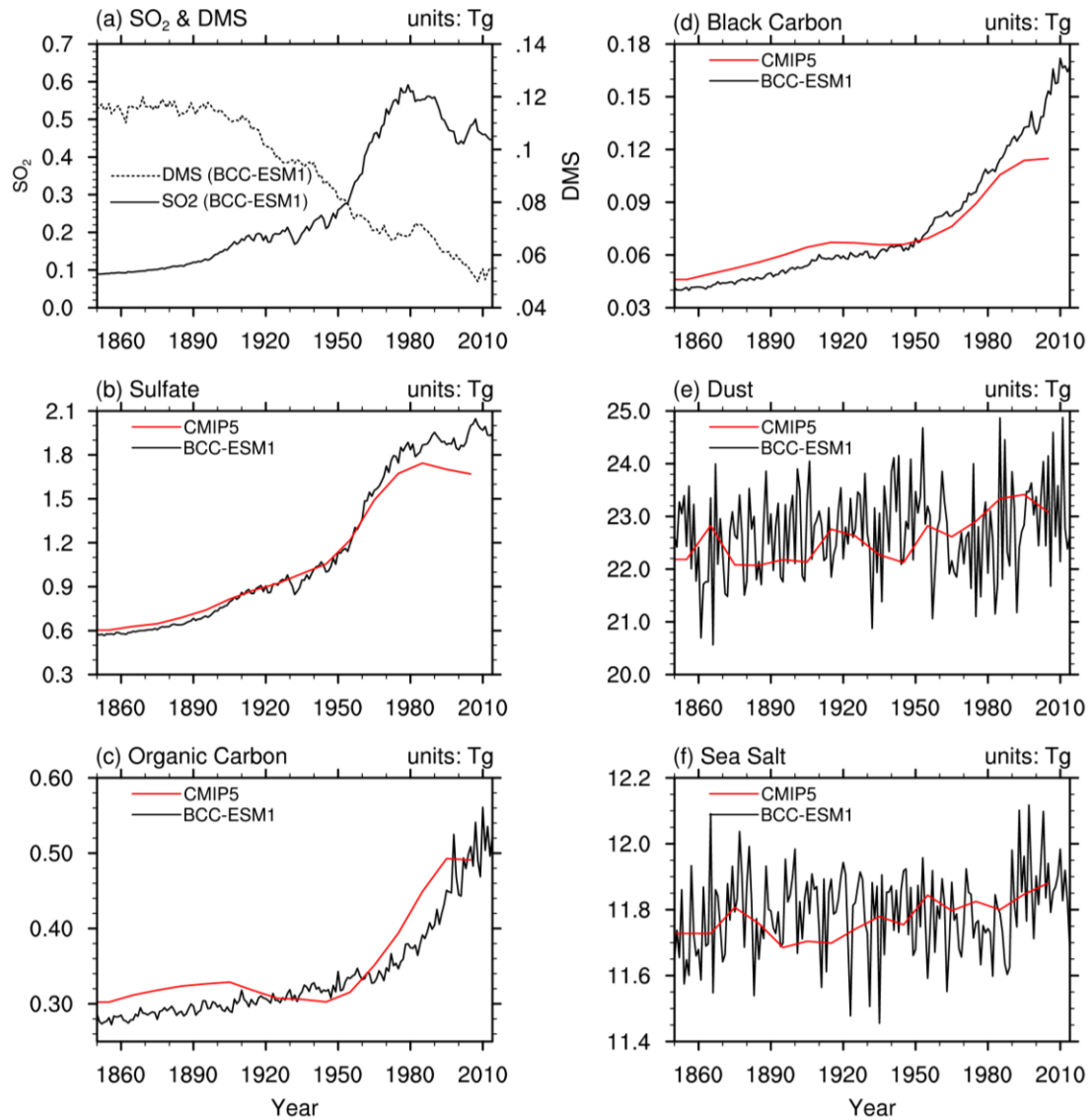


Figure 7. The time series of global yearly amounts of (a) SO₂ and DMS and (b-f) aerosols in the whole atmosphere column from the CMIP6 historical simulations of BCC-ESM1 (black lines) and the CMIP5-recommended aerosols masses (red lines). The yearly CMIP5 data are interpolated from the time series in 10-year interval. Units: Tg.

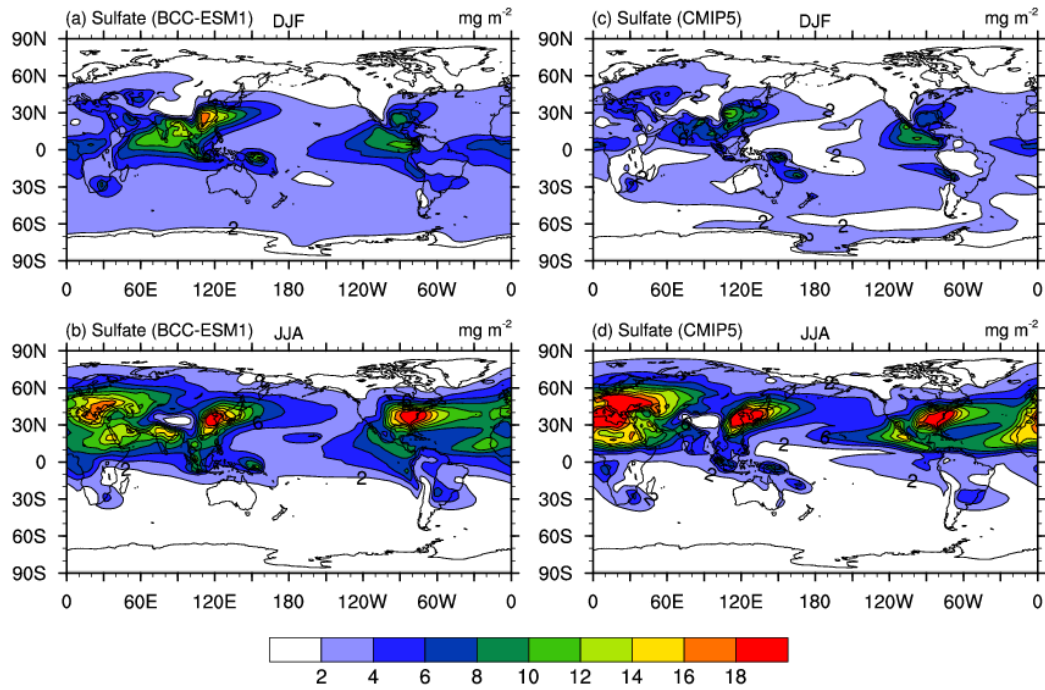


Figure 8. December-January-February (DJF; top panels) and June-July-August (JJA; bottom panels) mean sulfate (SO_4^{2-}) aerosol column mass concentrations averaged for the period of 1971-2000. Left panels show the historical simulations of BCC-ESM1, and right panels the CMIP5-recommended data. Units: mg.m^{-2} .

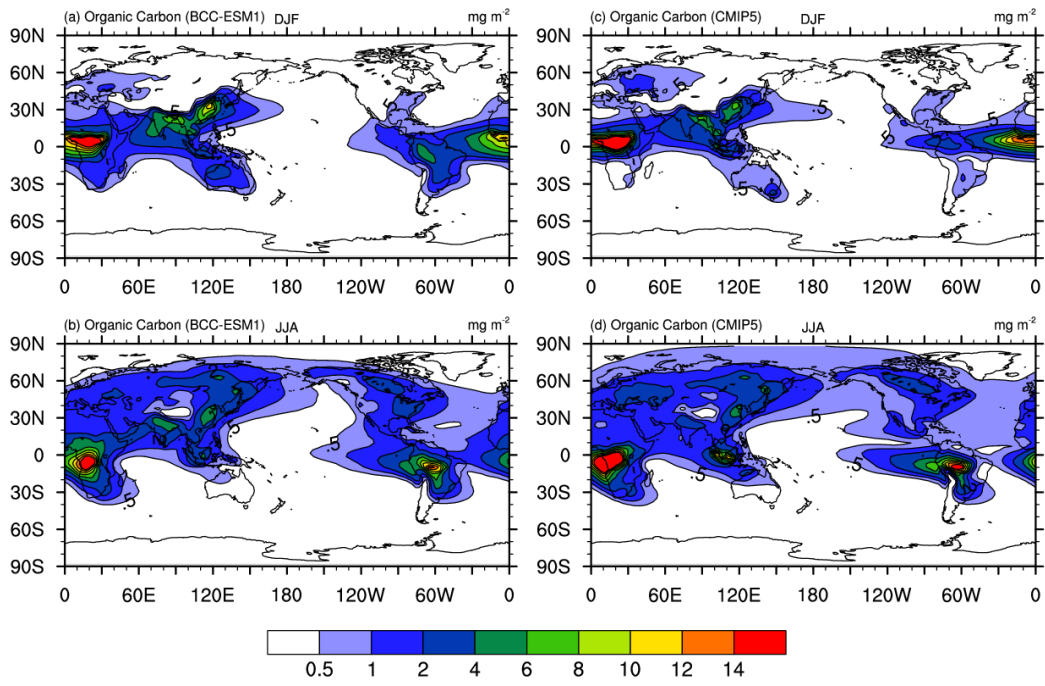


Figure 9. The same as in Figure 8, but for organic carbon (OC) aerosol column mass concentrations. Units: mg m^{-2} .

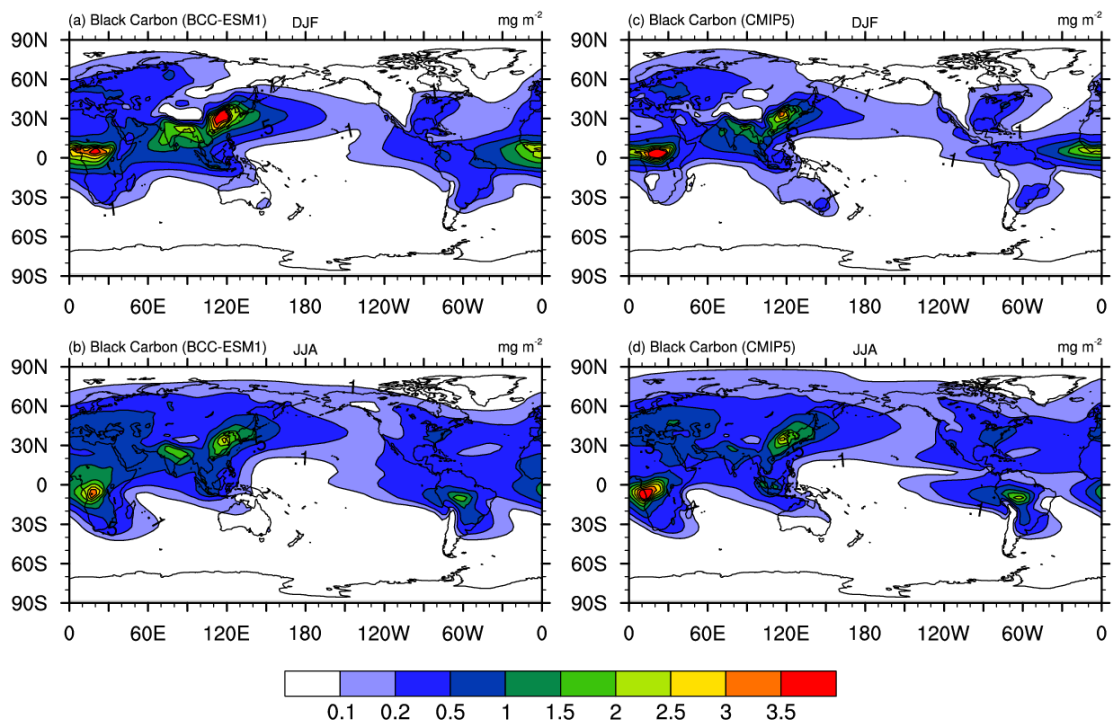


Figure 10. The same as in Figure 8, but for black carbon (BC) aerosol. Units: mg.m^{-2} .

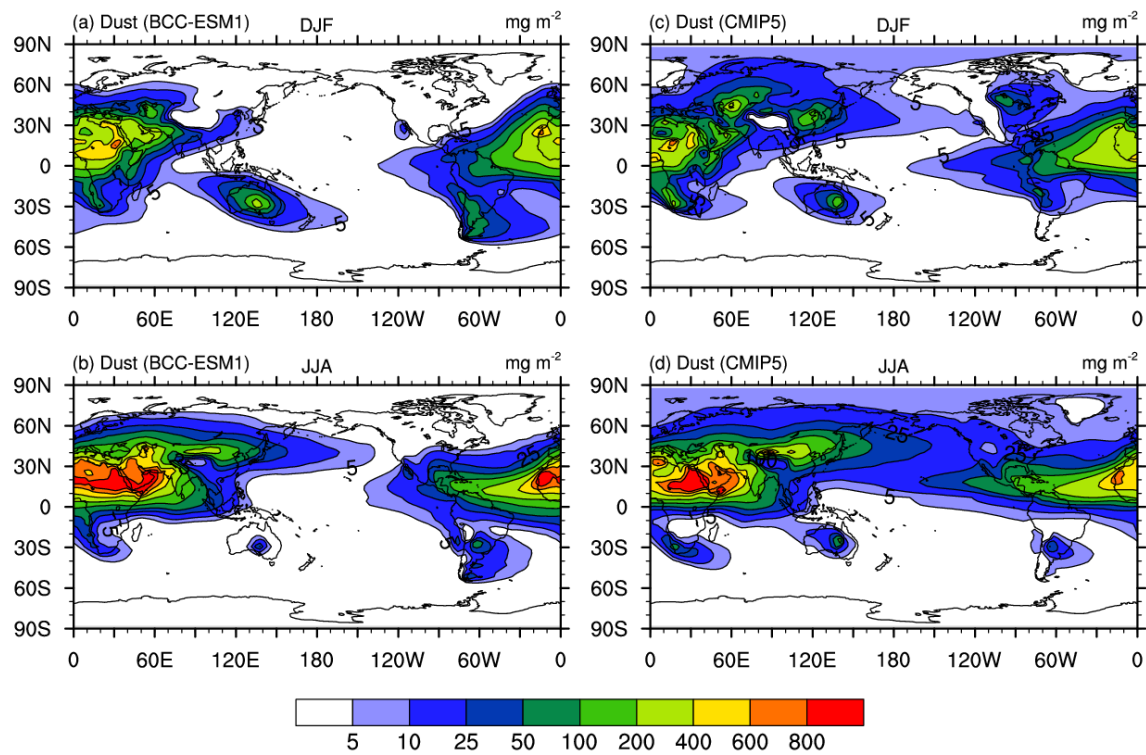


Figure 11. The same as in Figure 8, but for dust aerosol. Units: mg.m^{-2} .

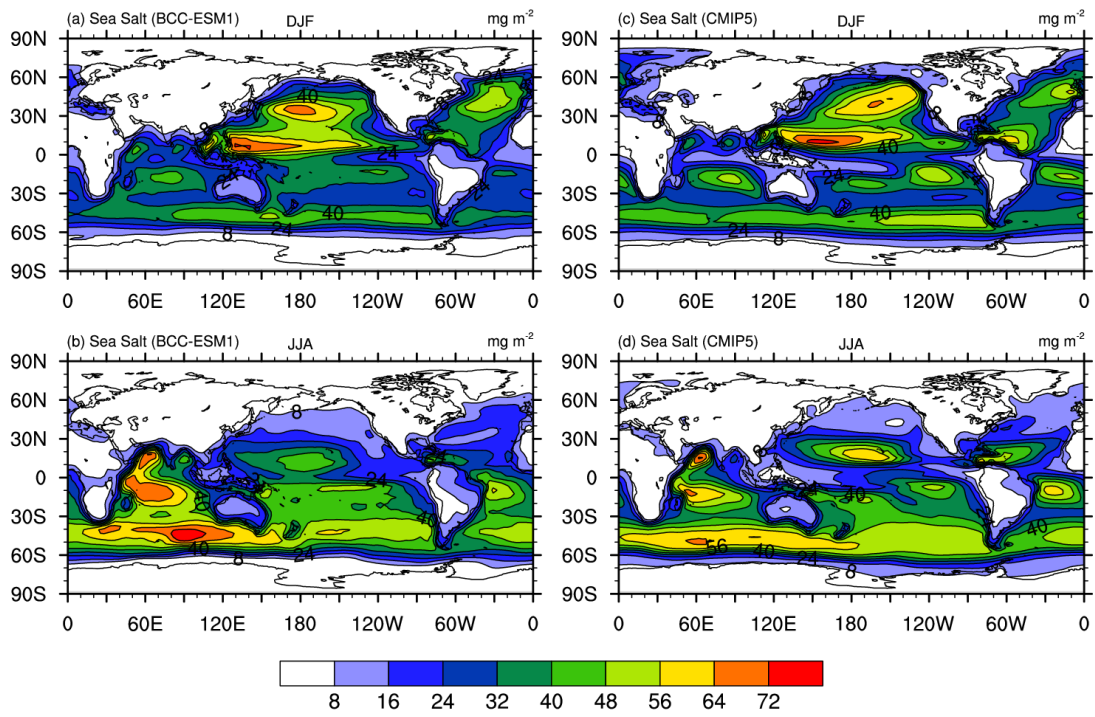


Figure 12. The same as in Figure 8, but for sea salt (SSLT) aerosol. Units: mg.m^{-2} .

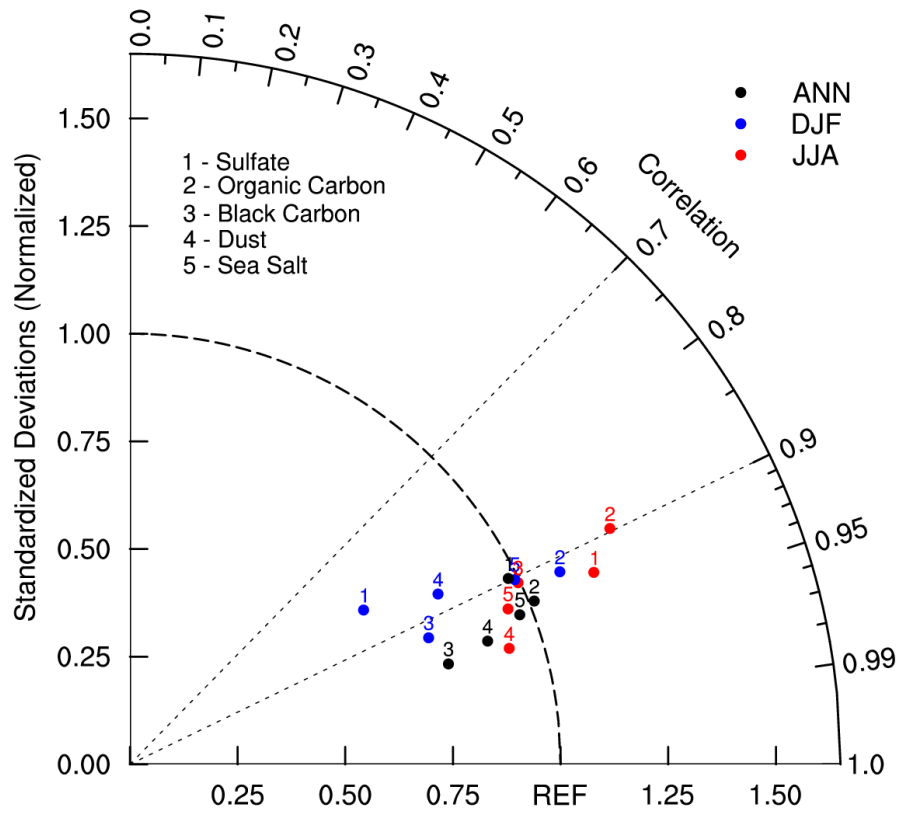


Figure 13. Taylor diagram for the global aerosols climatology (1971–2000) of sulfate, organic carbon, black carbon, dust, and sea salt averaged for December-January-February (DJF), June-July-August (JJA), and annual respectively. The radial coordinate shows the standard deviation of the spatial pattern, normalized by the observed standard deviation. The azimuthal variable shows the correlation of the modelled spatial pattern with the observed spatial pattern. Analysis is for the whole globe. The reference dataset is CMIP5-prescribed dataset.

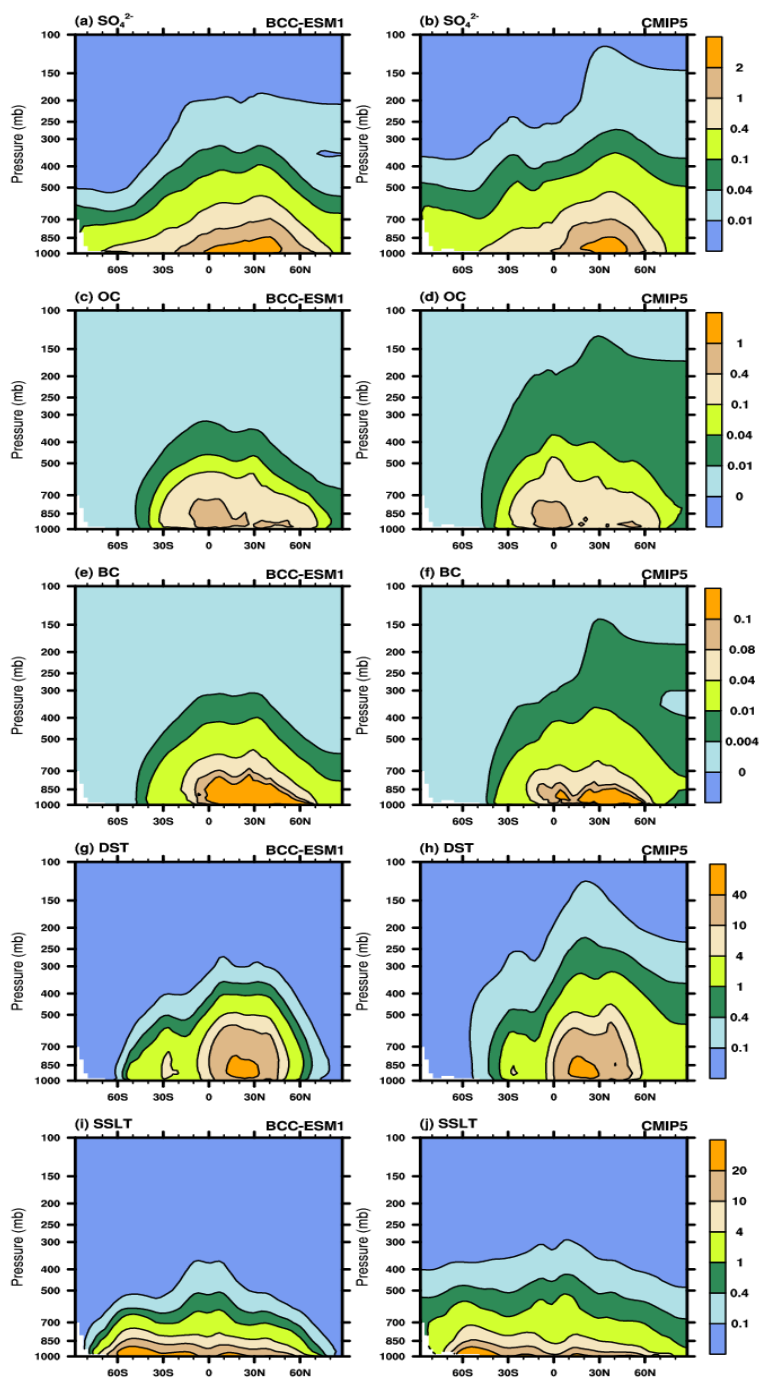


Figure 14. Latitude-pressure distributions of zonally-averaged annual mean sulfate, organic carbon, black carbon, dust, and sea salt aerosol concentrations for the period of 1971-2000. Left panels show the CMIP6 historical simulation of BCC-ESM1, and right panels the CMIP5 recommendation data. Units: $\mu\text{g m}^{-3}$.

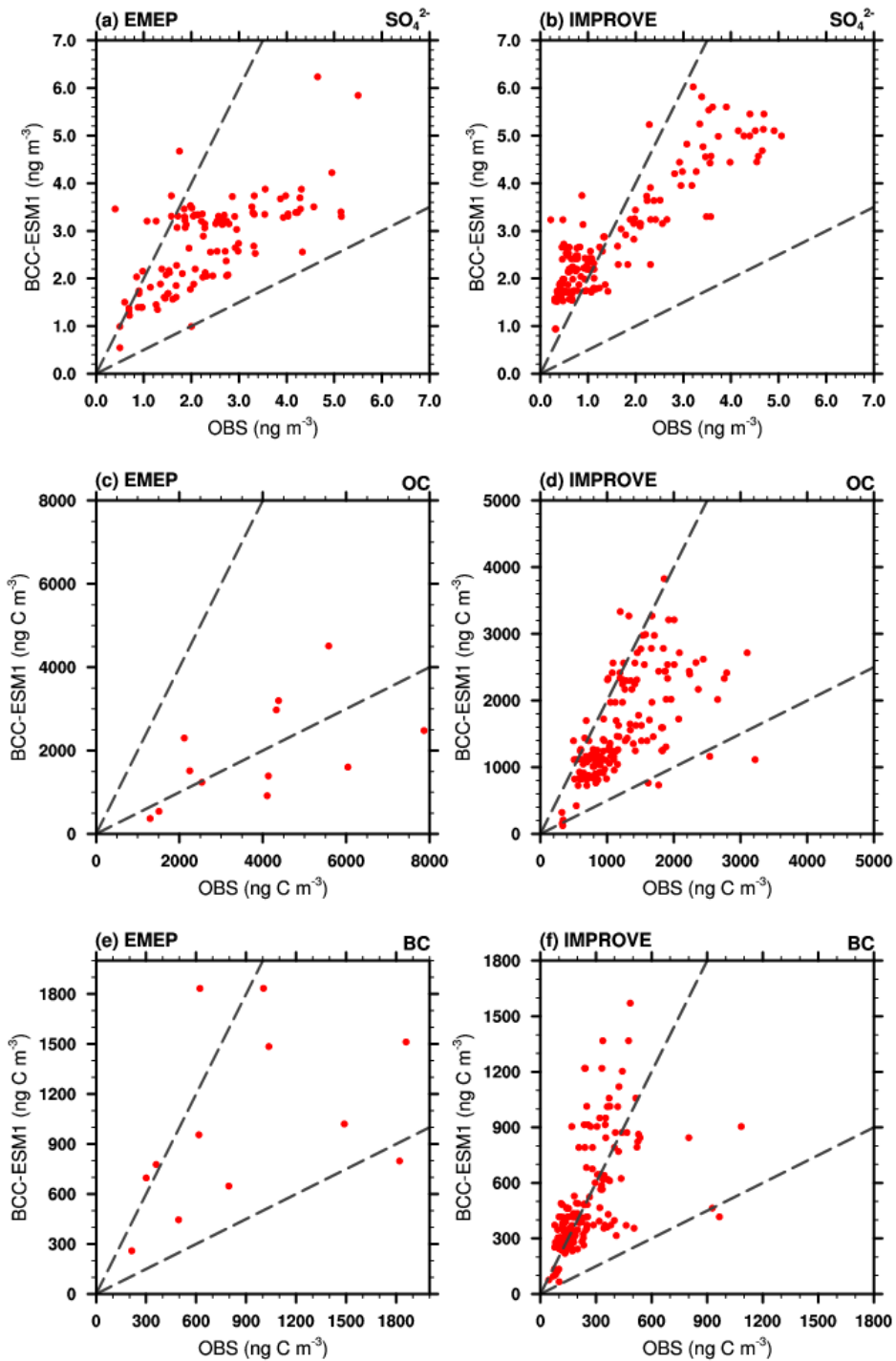


Figure 15. Scatter plots showing observed versus simulated multi-years averaged annual mean sulfate (SO_4^{2-}), organic carbon (OC), black carbon (BC) mixing ratios at IMPROVE and EMEP network sites. Observations are averages over the available years 1990–2005 for IMPROVE sites, and 1995–2005 for EMEP sites. Simulated values are those at the lowest layer of BCC-ESM1.

Table 7. Observed versus simulated concentrations of sulfate (SO_4^{2-}), organic carbon (OC), black carbon (BC) for the regional mean and spatial standard deviation, minimum and maximum values at [HIPPO aircraft observations \(BC only\)](#), IMPROVE and EMEP network sites, and the spatial correlation between observed and simulated multi-years averaged annual means. Simulated values are selected for the same locations and same valid observation time. The data used same as those in Figure 12.

	EMEP			IMPROVE			HIPPO
	SO_4^{2-} (Obs/Model)	OC (OBS/Model)	BC (OBS/Model)	SO_4^{2-} (OBS/Model)	OC (OBS/Model)	BC (OBS/Model)	<u>BC (OBS/Model)</u>
Mean Values	2.37/2.74	3844/1919	884/1022	1.53/2.79	1215/1565	249/504	<u>8.2/11.1</u>
Std Deviation	1.16/0.93	1997/1215	572/526	1.30/1.20	572/745	164/296	<u>27.9/21.0</u>
Min Values	0.40/0.55	1296/369	214/259	0.22/0.94	322/123	45/66	<u>0.0025/0.066</u>
Max Values	5.50/6.24	7867/4510	1859/1834	5.07/6.02	3219/3827	1084/1570	<u>558.91/267.11</u>
Correlation (Obs and Model)	0.67	0.56	0.40	0.90	0.63	0.55	<u>0.51</u>

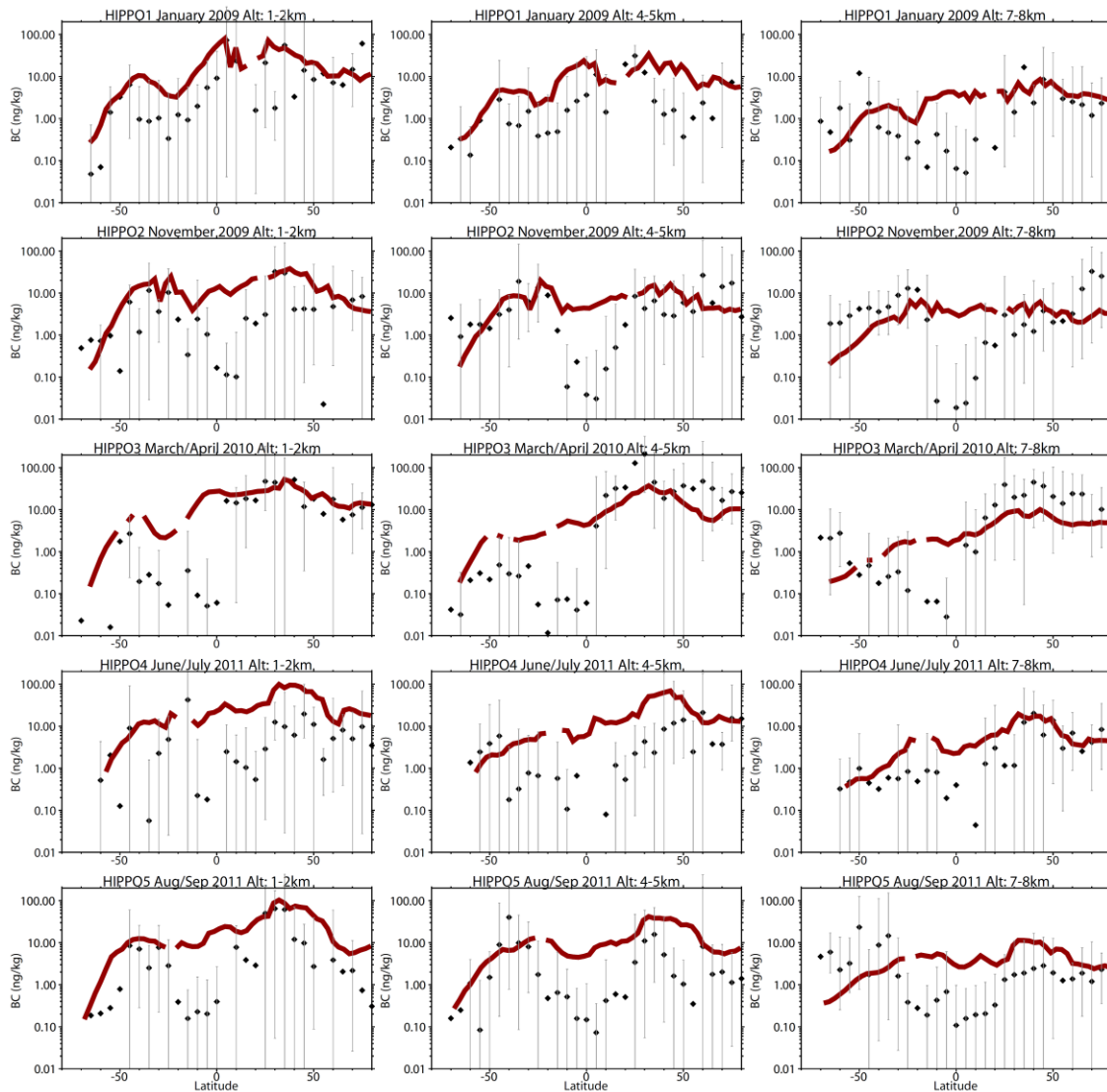


Figure 16. Comparison of modelled black carbon (BC) aerosol (red lines) with observations from HIPPO aircraft campaigns over the Pacific Ocean (black symbols, bars represent the full data range). Observations from different HIPPO campaigns were averaged over 5 °latitude bins and three different altitude bands (left column: 1-2 km, middle column: 4-5 km, and right column: 7-8 km) along the flight track over the Pacific Ocean. Model results were sampled along the flight track and then averaged over the abovementioned regions for comparison.

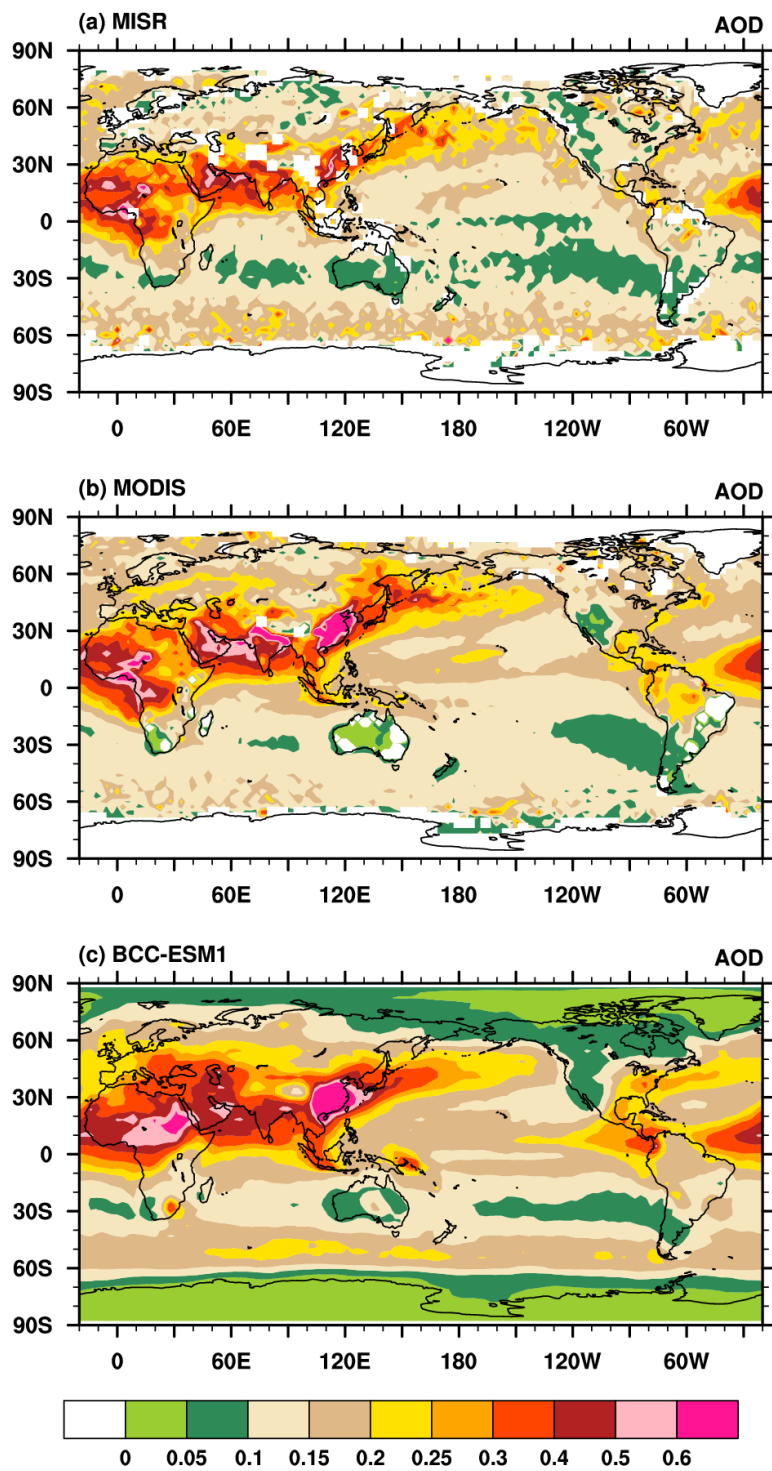


Figure 17. Global distribution of annual mean AOD simulated in BCC-ESM1 compared with the MISR and MODIS data for the year 2008.

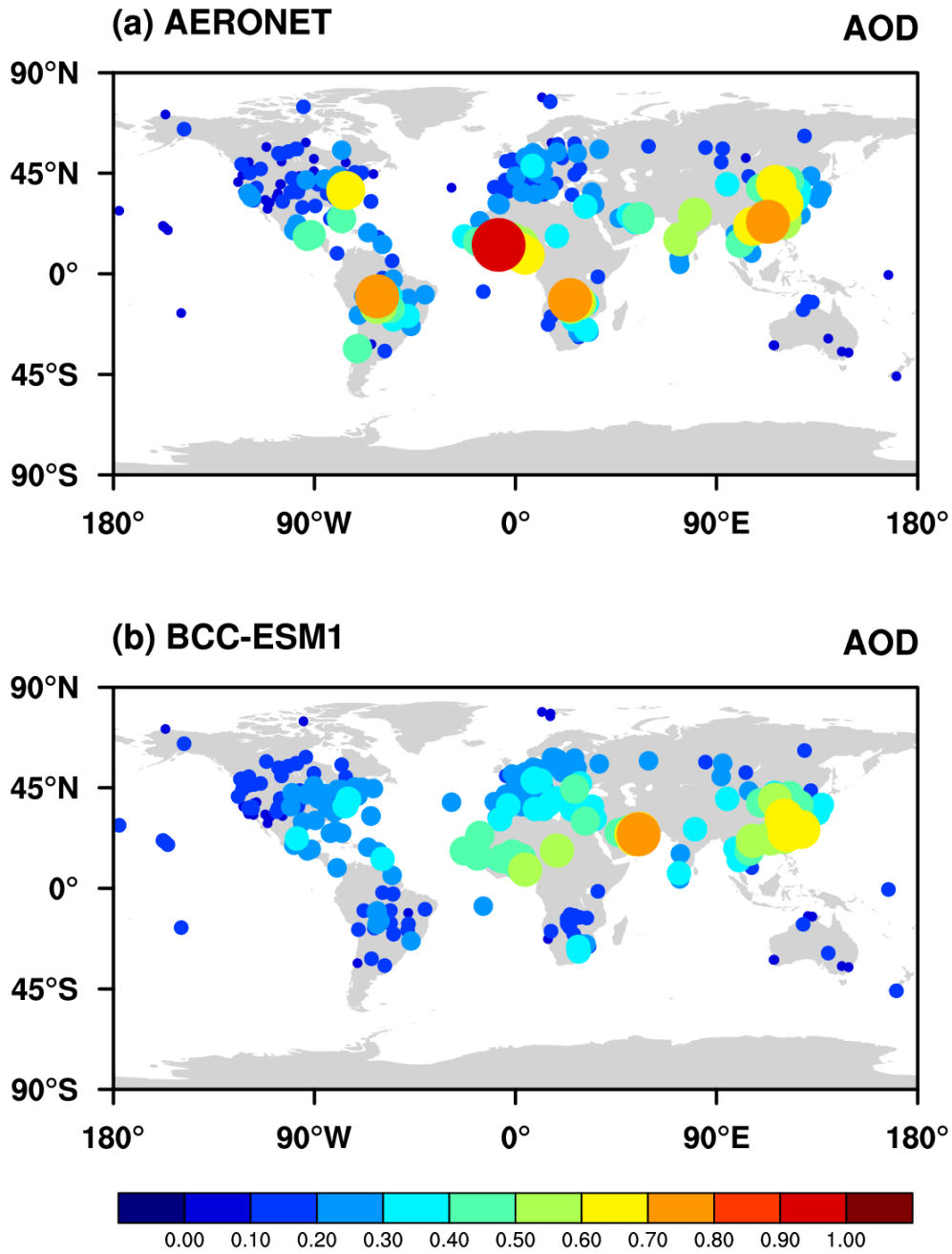


Figure 18. Observed versus simulated annual means of AOD at AERONET sites. Each data point represents the mean averaged for available monthly values of AOD. The dot sizes denote the magnitudes of AOD at sites. The spatial correlation is 0.56.

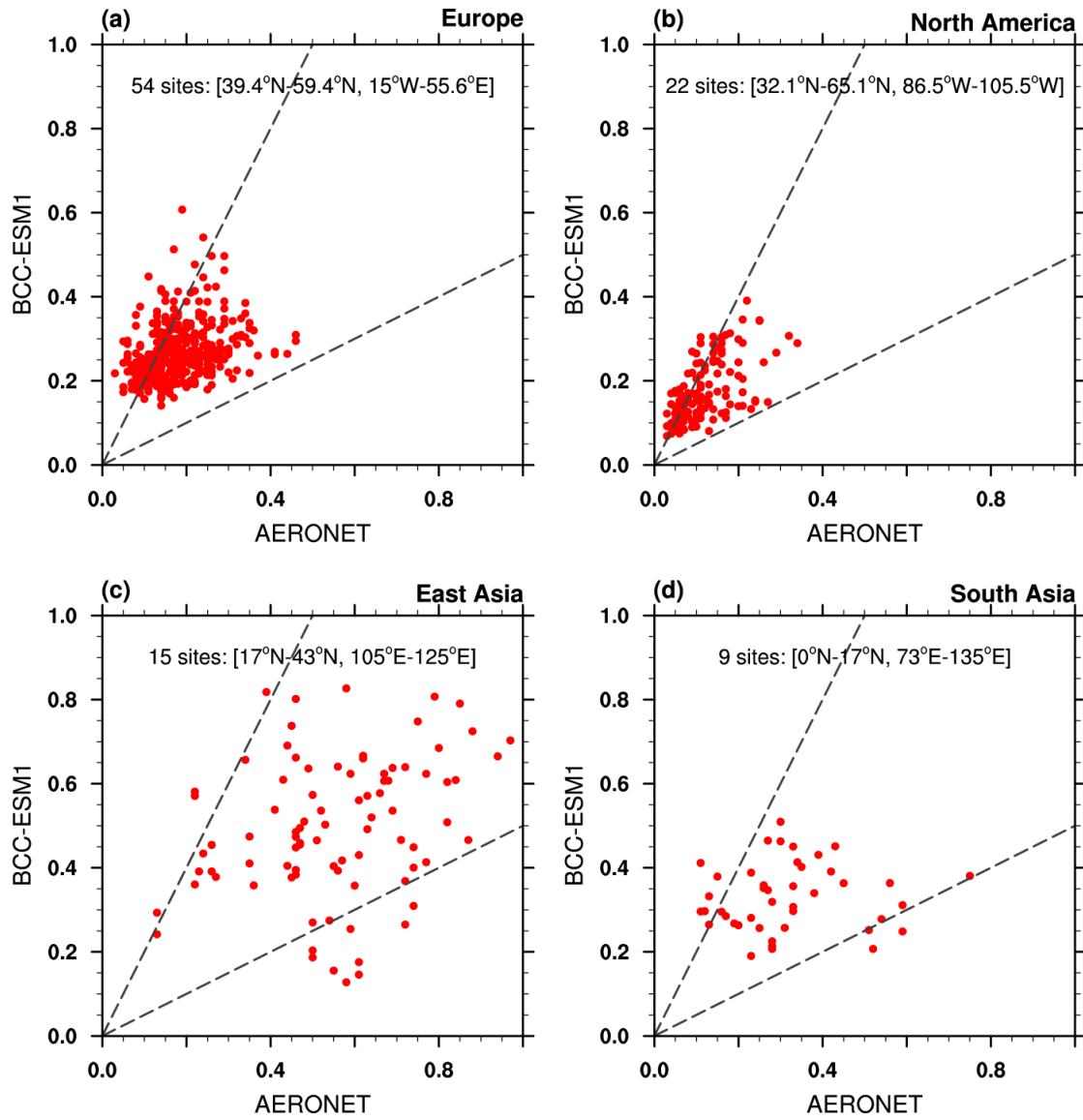


Figure 19. Scatter plots of observed versus simulated monthly mean AOD at AERONET sites in Europe, North America, East Asia, and South Asia over the period of 1998-2005.